THE NASA ATMOSPHERIC TOMOGRAPHY (ATom) MISSION: Imaging the Chemistry of the Global Atmosphere

BAMS Article

The NASA Atmospheric Tomography (ATom) Mission

Imaging the Chemistry of the Global Atmosphere

Chelsea R. Thompson, Steven C. Wofsy, Michael J. Prather, Paul A. Newman, Thomas F. Hanisco, Thomas B. Ryerson, David W. Fahey, Eric C. Apel, Charles A. Brock, William H. Brune, Karl Froyd, Joseph M. Katich, Julie M. Nicely, Jeff Peischl, Eric Ray, Patrick R. Veres, Siyuan Wang, Hannah M. Allen, Elizabeth Asher, Huisheng Bian, Donald Blake, Ilann Bourgeois, John Budney, T. Paul Bui, Amy Butler, Pedro Campuzano-Jost, Cecilia Chang, Mian Chin, Róisín Commane, Gus Correa, John D. Crounse, Bruce Daube, Jack E. Dibb, Joshua P. DiGangi, Glenn S. Diskin, Maximilian Dollner, James W. Elkins, Arlene M. Fiore, Clare M. Flynn, Hao Guo, Samuel R. Hall, Reem A. Hannun, Alan Hills, Eric J. Hintsa, Alma Hodzic, Rebecca S. Hornbrook, L. Greg Huey, Jose L. Jimenez, Ralph F. Keeling, Michelle J. Kim, Agnieszka Kupc, Forrest Lacey, Leslie R. Lait, Jean-Francois Lamarque, Junhua Liu, Kathryn McKain, Simone Meinardi, David O. Miller, Stephen A. Montzka, Fred L. Moore, Eric J. Morgan, Daniel M. Murphy, Lee T. Murray, Benjamin A. Nault, J. Andrew Neuman, Louis Nguyen, Yenny Gonzalez, Andrew Rollins, Karen Rosenlof, Maryann Sargent, Gregory Schill, Joshua P. Schwarz, Jason M. St. Clair, Stephen D. Steenrod, Britton B. Stephens, Susan E. Strahan, Sarah A. Strode, Colm Sweeney, Alexander B. Thames, Kirk Ullmann, Nicholas Wagner, Rodney Weber, Bernadett Weinzierl, Paul O. Wennberg, Christina J. Williamson, Glenn M. Wolfe, and Linghan Zeng

ABSTRACT: This article provides an overview of the NASA Atmospheric Tomography (ATom) mission and a summary of selected scientific findings to date. ATom was an airborne measurements and modeling campaign aimed at characterizing the composition and chemistry of the troposphere over the most remote regions of the Pacific, Southern, Atlantic, and Arctic Oceans, and examining the impact of anthropogenic and natural emissions on a global scale. These remote regions dominate global chemical reactivity and are exceptionally important for global air quality and climate. ATom data provide the in situ measurements needed to understand the range of chemical species and their reactions, and to test satellite remote sensing observations and global models over large regions of the remote atmosphere. Lack of data in these regions, particularly over the oceans, has limited our understanding of how atmospheric composition is changing in response to shifting anthropogenic emissions and physical climate change. ATom was designed as a global-scale tomographic sampling mission with extensive geographic and seasonal coverage, tropospheric vertical profiling, and detailed speciation of reactive compounds and pollution tracers. ATom flew the NASA DC-8 research aircraft over four seasons to collect a comprehensive suite of measurements of gases, aerosols, and radical species from the remote troposphere and lower stratosphere on four global circuits from 2016 to 2018. Flights maintained near-continuous vertical profiling of 0.15–13-km altitudes on long meridional transects of the Pacific and Atlantic Ocean basins. Analysis and modeling of ATom data have led to the significant early findings highlighted here.

KEYWORDS: Aerosols/particulates; Aircraft observations; Atmospheric composition; Atmospheric oxidation; Model evaluation/performance; Seasonal variability

https://doi.org/10.1175/BAMS-D-20-0315.1
Corresponding author: Chelsea R. Thompson, chelsea.thompson@noaa.gov
Supplemental material: https://doi.org/10.1175/BAMS-D-20-0315.2

In final form 30 September 2021

AFFILIATIONS: Thompson, Froyd, Katich, Peischl, Ray, Bourgeois, Neuman, Schill, Wagner, and Williamson—NOAA Chemical Sciences Laboratory, and University of Colorado Boulder, Boulder, Colorado; **Ryerson, Fahey, Brock, Veres, Butler, Murphy, Rollins, Rosenlof, and Schwarz**—NOAA Chemical Sciences Laboratory, Boulder, Colorado; **Wofsy, Budney, Commane,* Daube, Gonzalez, and Sargent**—Harvard University, Cambridge, Massachusetts; **Prather, Blake, Flynn,* Guo, and Meinardi**—University of California, Irvine, Irvine, California; **Newman, Hanisco, Chin, and Wolfe**—NASA Goddard Space Flight Center, Greenbelt, Maryland; **Nicely**—NASA Goddard Space Flight Center, Greenbelt, and University of Maryland, College Park, College Park, Maryland; **Apel, Wang,* Asher,* Hall, Hills, Hodzic, Hornbrook, Lacey, Lamarque, Stephens, and Ullmann**—National Center for Atmospheric Research, Boulder, Colorado; **Brune, Miller, and Thames**—The Pennsylvania State University, University Park, Pennsylvania; **Allen, Crounse, Kim, and Wennberg**—California Institute of Technology, Pasadena, California; **Bian, Hannun, and St. Clair**—NASA Goddard Space Flight Center, Greenbelt, and University of Maryland, Baltimore County, Baltimore, Maryland; **Bui and Chang**—NASA Ames Research Center, Mountain View, California; **Campuzano-Jost, Jimenez, and Nault***—University of Colorado Boulder, Boulder, Colorado; **Correa and Fiore**—Columbia University, Palisades, New York; **Dibb**—University of New Hampshire, Durham, New Hampshire; **DiGangi, Diskin, and Nguyen**—NASA Langley Research Center, Hampton, Virginia; **Dollner and Weinzierl**—University of Vienna, Vienna, Austria; **Elkins, Montzka, and Sweeney**—NOAA Global Monitoring Laboratory, Boulder, Colorado; **Hintsa, McKain, and Moore**—NOAA Global Monitoring Laboratory, and University of Colorado Boulder, Boulder, Colorado; **Huey, Weber, and Zeng**—Georgia Institute of Technology, Atlanta, Georgia; **Keeling and Morgan**—Scripps Institution of Oceanography, La Jolla, California; **Kupc**—NOAA Chemical Sciences Laboratory, Boulder, Colorado, and University of Vienna, Vienna, Austria; **Lait**—NASA Goddard Space Flight Center, Greenbelt, and Science Systems and Applications, Inc., Lanham, Maryland; **Liu, Steenrod, Strahan, and Strode**—NASA Goddard Space Flight Center, Greenbelt, and Universities Space Research Association, Columbia, Maryland; **Murray**—University of Rochester, Rochester, New York
CURRENT AFFILIATIONS: Commane—Columbia University, Palisades, New York; **Flynn**—Stockholm University, Stockholm, Sweden; **Wang and Asher**—NOAA Chemical Sciences Laboratory, and University of Colorado Boulder, Boulder, Colorado; **Nault**—Aerodyne Research Inc., Billerica, Massachusetts

The NASA Atmospheric Tomography (ATom) mission was a global-scale airborne campaign, flying over four seasons from August 2016 to May 2018, and funded through the NASA Earth Venture Suborbital-2 (EVS-2) program. ATom addresses gaps in our understanding of chemical composition, reactivity, and transport in the remote troposphere. Observations collected during ATom provide unique information to test and improve global chemistry–transport and chemistry–climate models (CTMs, CCMs) and to test and improve satellite retrievals of chemical species over the oceans.

The ATom mission was intensive in its comprehensive measurement of atmospheric composition and extensive in its spatial and temporal sampling. ATom utilized the fully instrumented NASA DC-8 research aircraft to collect a broad suite of measurements of gases, aerosols, aerosol formation and evolution, meteorological parameters, and key radical species from the remote troposphere and lower stratosphere. Four complete nearly pole-to-pole global circuits (one in each season) were conducted; each circuit included long meridional transects of the Pacific and Atlantic Ocean basins as well as transects across the Southern Ocean and the Arctic. These flights resulted in an unprecedented dataset (archived at https://doi.org/10.3334/ORNLDAAC/1581) that characterize the chemical state of the whole troposphere as well as the human imprint on the most remote parts of it. Data from ATom can provide the information

needed to improve our understanding of chemical transformations and long-range transport of pollutants in that vast part of the atmosphere that we often designate as "background." The ATom dataset provides new categories of tests for global CCMs, with a particular focus on data-constrained rates of ozone (O_3) production and loss, methane (CH_4) loss, statistical distributions of species driving these rates, and their links to distant pollution.

The distribution and atmospheric fate of short-lived climate forcers (SLCFs), notably CH_4, O_3, aerosols [in particular black carbon (BC)], and hydrofluorocarbons (HFCs), are prime foci of the ATom mission. The SLCFs also include pollutants such as NO and CO that indirectly force climate by altering the chemical rates controlling concentrations of CH_4, HFCs, and O_3. SLCFs collectively are powerful climate forcers responsible for up to 45% (Myhre et al. 2013) of current warming caused by human activities, as well as key pollutants impacting global air quality (Fleming et al. 2018; Gaudel et al. 2018; Scovronick et al. 2015; Zaelke 2013; Zhang et al. 2016). Due to their shorter atmospheric residence times relative to that of carbon dioxide (CO_2), reductions in several of these species offer potential to slow the rate of warming and dampen the near-term impacts of climate change. Methane, in particular, has been the focus of much attention due its potency as a greenhouse gas and its importance in controlling the abundance of tropospheric O_3 (Fiore et al. 2012; Kirtman et al. 2013; West et al. 2006). The greater than twofold rise in atmospheric CH_4 from preindustrial to present levels is responsible for nearly half of the increase in the tropospheric O_3 burden over the same time period (Myhre et al. 2013; Prather et al. 2001). These species have been recognized as key targets in international efforts to mitigate the effects of climate change while simultaneously improving air quality (Anenberg et al. 2012; Fiore et al. 2012; Hansen et al. 2000; Shindell et al. 2011, 2012a; Velders et al. 2009).

To evaluate the impacts of human pollution on climate and air quality, as well as plan a scientifically based mitigation strategy, it is necessary to understand the chemical state of the current atmosphere so that we can predict the consequence of changes in anthropogenic emissions on the climate (e.g., temperature, convection, lightning, oceanic and other natural emissions). The ATom mission specifically focused on characterizing the remote atmosphere over the largest ocean basins, which are distant from, but still influenced by, anthropogenic pollution (Crawford et al. 2004; Fishman et al. 1990, 1991; Fried et al. 2008; Heald et al. 2003; Singh et al. 2009; Watson et al. 1990; Wofsy 2011). These oceanic regions are important for global air quality and climate, accounting on average for an estimated 75% of global CH_4 removal, 59% of chemical production of tropospheric O_3, and 68% of chemical destruction of tropospheric O_3; these chemical reactivities are particularly sensitive to changes in the intensity and spatial distribution of pollutant emissions (Holmes et al. 2013; Zhang et al. 2016). In situ measurements have been historically sparse over the remote oceans, owing to the great distance to be covered and the logistical difficulties and expense of such campaigns. A few remote surface sites have provided information to address some of these questions, but they have not included the breadth of measurements provided by the ATom mission (Ayers et al. 1996; Helmig et al. 2008; Liu et al. 1992; Monks et al. 1998; Read et al. 2012; Schum et al. 2018).

A significant value of the ATom dataset lies in its capacity to inform and constrain the global CCMs that serve as the principal tools for the Intergovernmental Panel on Climate Change (IPCC) assessments (Kirtman et al. 2013; Lamarque et al. 2013). Although significant advances have been made in developing these CCMs, there continue to be large differences in fundamental model diagnostics. For example, the atmospheric lifetime of CH_4 calculated in CCMs ranges from 7 to 14 years with no clear information on what causes this large range (Holmes et al. 2013; IPCC 2022; Naik et al. 2013; Prather et al. 2012; Voulgarakis et al. 2013). A persistent weakness in these CCM comparisons lies in the lack of critical tests for the current chemical and microphysical state of the atmosphere, particularly in the remote atmosphere (Schwarz et al. 2013; Shindell et al. 2012b; Tsigaridis et al. 2014; Young et al. 2013). Numerous model intercomparison projects (MIPs) over the years have shown that, even when initiated

with a standardized set of emissions, different CCMs can generate very different realizations of atmospheric chemistry and reactivity (Emmons et al. 2015; Lamarque et al. 2013; Prather et al. 2018). Fortunately, ATom now provides, for the first time, a statistical distribution of most of the critical reactive gases and aerosols, including their covariance and the derived photochemical reactivities, with which to confront the CCMs chemical climatologies.

This article provides a description of the ATom project, including the mission goals and objectives, project design and flight strategy, and a summary of the meteorological and climatological conditions encountered on the four deployments. An early view of results here highlights some of the major outcomes of the mission and summarizes scientific findings from the first published papers. Further information on the mission and a current list of ATom publications can be found at the mission website (https://espo.nasa.gov/atom) and access to the ATom datasets is available through the long-term data archive (https://doi.org/10.3334/ORNLDAAC/1925).

Context with previous studies

The NASA ATom mission builds upon a foundation of previous airborne missions focused on remote ocean regions, such as the NASA Global Tropospheric Experiment Program (GTE, 1983–2001), the NASA Intercontinental Chemical Transport Experiment–Phase B (INTEX-B/Part II, 2006), and the NSF High-Performance Instrumented Airborne Platform for Environmental Research (HIAPER) Pole-to-Pole Observations (HIPPO, 2009–11). These are summarized in Table ES1 and Fig. ES1 in the online supplemental material.

The GTE program pioneered large-scale airborne atmospheric chemistry studies in remote areas and encompassed several series of campaigns that utilized the NASA DC-8 aircraft to study the chemistry and composition of the troposphere and the impacts of anthropogenic emissions in the remote atmosphere over the Pacific and Atlantic Oceans (Fishman et al. 1996; McNeal et al. 1998). The GTE campaigns met their scientific objectives by targeting particular airmass types in geographically focused regions of interest. More recently, the HIPPO campaign deployed the NSF/NCAR Gulfstream V aircraft for a series of five pole-to-pole missions flying north–south transects of the Pacific Ocean basin (Wofsy 2011). HIPPO demonstrated the feasibility and advantages of global-scale tomographic flights that would be used for the ATom mission. Due to the limited payload capacity of the Gulfstream V, the HIPPO payload was restricted to measurements of greenhouse gases, BC, O_3, H_2O, peroxyacyl nitrates (PAN), and halocarbons.

The ATom mission merged the tomographic, survey-style sampling of HIPPO with the comprehensive instrument payload afforded by the DC-8 and extended the research region from the Pacific to also include the Atlantic Ocean basin, the Southern Ocean, and the Arctic Ocean. ATom included all variables measured during HIPPO, providing a repeat snapshot of the Pacific to enable detection of decadal changes. ATom leveraged the significant analytical measurement advances that have been achieved since the GTE campaigns with an updated suite of aircraft instruments and data from new satellite sensors that were not available during the GTE and HIPPO campaigns.

Mission objectives and strategy

The primary scientific goals of ATom were to (i) develop an observation-based measure of the atmospheric production and destruction of O_3, and the removal of CH_4 and BC across global scales, (ii) establish critical metrics of these processes to test CTMs and CCMs, and (iii) provide critical data for satellite remote sensing algorithm development and testing. Central to these goals were seven key scientific objectives:

1) Quantify the processes and rates controlling CH_4, O_3, and BC abundances in the atmosphere.
2) Determine how remote CH_4, O_3, and BC are affected by urban, industrial, agricultural, and natural emissions from major source regions.

Table 1. Defining characteristics of the ATom mission strategy.

Defining characteristics of the ATom mission strategy	
Comprehensive measurement payload	In situ measurements were made of reactive and long-lived gases, radical precursors, key radical species, aerosols and aerosol properties, radiation, and meteorological parameters.
Tomographic, global-scale sampling	Continuous airborne profiling was performed from near-surface to ~13-km altitude along pole-to-pole flight tracks in the Pacific and Atlantic Ocean basins and across the Southern and Arctic Oceans.
Objective sampling	ATom came as close as possible to achieving a representative ensemble of the background atmosphere by objectively sampling along predefined transects rather than targeting specific air masses.
Focus on the remote atmosphere	Flight transects were performed over the remote oceans where in situ observations have been historically sparse.
Daytime flights	Flight times were chosen to maximize solar radiation to evaluate photochemistry and test photochemical models.
Repeated deployments	Four complete global circuits were performed in the four different seasons to investigate the seasonal variability in composition and reactivity.
Complete investigation	A holistic approach was employed that incorporated chemical and physical measurements, meteorology, photochemical and transport modeling, and satellite validation.

3) Determine the large-scale distributions and size spectra of different aerosol species.
4) Infer the mechanisms primarily responsible for new particle formation in the remote atmosphere.
5) Determine how aging affects aerosol removal from the atmosphere.
6) Measure greenhouse gases and ozone-depleting substances remote from sources to help identify and constrain anthropogenic sources and global budgets.
7) Conduct numerous vertical profiles to quantify bias and errors of satellite retrievals and to assimilate satellite data into ATom analyses.

To achieve these goals, ATom employed a unique mission strategy with several defining characteristics, as outlined in Table 1.

The comprehensive instrument payload focused on high-time-resolution measurements of the SLCFs and reactive trace gases that serve as important radical precursors, plus the key radical species and photolysis rates that drive photochemistry, complemented by extensive flask measurements. Flight times were strategically chosen to maximize solar radiation (i.e., centered on daylight hours to the extent possible) to capture the peak in photochemical activity, and were required for optimal profiling.

ATom collected an objective and representative ensemble of measurements of the background atmosphere by flying long, tomographic transects across the remote oceans along repeated, predefined flight tracks that avoided targeting any particular airmass types. The term tomography refers to a method of generating thin cross sections for imaging applications. In practice, a tomographic flight pattern employs repeated and systematic vertical profiles along a transect to create a curtain of observations along a defined distance (on the *x* axis) and within a defined altitude range (on the *y* axis). ATom transects spanned an altitude range of 0.15–13 km and reached nearly pole-to-pole meridionally down the center of the Pacific and Atlantic Ocean basins and zonally across the Arctic and Southern Oceans. A third meridian was also flown in the tropical east Pacific to capture systematic differences in O_3 between the central and eastern Pacific associated with the Walker circulation (Oman et al. 2011) and the North American monsoon, and two flights extended into the Antarctic continent. Nearly identical flight tracks were flown on four complete deployments that occurred in each of the four seasons to capture the annual variation of natural and anthropogenic sources, transport, and atmospheric sinks.

Figure 1 identifies the major emissions sources and atmospheric processes involving land and oceans that ATom was designed to investigate. The ATom observations define the chemical

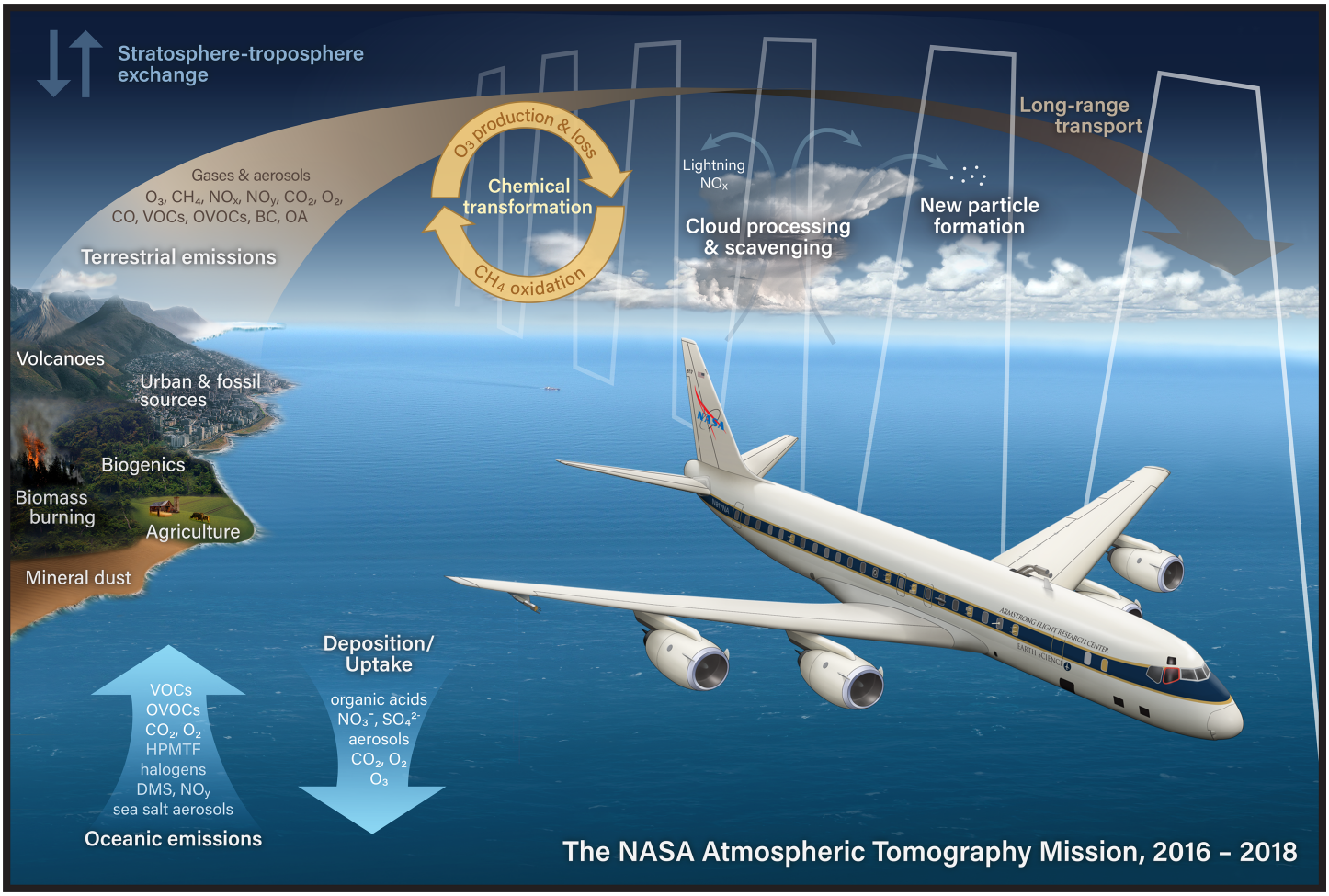

Fig. 1. Schematic illustration of the NASA ATom mission, highlighting the major emissions sources and atmospheric processes sampled during the deployments.

and microphysical state of the atmosphere for comparison to models in terms of both probability distributions and as specific realizations at the time of the observations (i.e., a test of chemical forecasts; Strode et al. 2018). While these ATom data are not a climatology in the sense of multiyear daily observations, they do provide a detailed statistical picture of the global atmosphere that is sampled unconditionally, intended to be a broadly representative ensemble.

The question of representativeness in comparison with CCM climatologies can be addressed directly using the models themselves. For example, Prather et al. (2017) showed that the joint probability distribution of NO_x and HOOH from a single transect accurately described the entire tropical Pacific for several models, and detailed comparisons have been made to the distributions of actinic irradiance (Hall et al. 2018). The strength of the ATom dataset for model evaluation lies in joint probability distributions across multiple species that is linked to the reactivity of the air parcels.

ATom global snapshots show the integrated effects of continental outflow from a range of anthropogenic and natural sources, including combustion and fossil fuel usage, agriculture, biomass burning, volcanoes, and desert dust, in addition to oceanic emissions and deposition. It was anticipated that the ATom mission would encounter distinct plumes of pollution and stratospheric intrusions in both oceans, representing the high-end tails of some probability distributions. The systematic, unbiased sampling pattern in ATom ensured characterization of the "background" median and high/low tail distributions, as well. This flight strategy was informed by experience from the HIPPO campaign, which transected the Pacific twice within a month, demonstrating that probability distributions of short-lived species are very similar

for repeated transects performed two weeks apart and that statistical distributions over long latitudinal transects are relatively insensitive to episodic transport events (Wofsy 2011).

Mission implementation and details

Platform and payload. The ATom mission utilized the NASA DC-8 Airborne Science Laboratory research aircraft based at NASA's Armstrong Flight Research Center (AFRC) in Palmdale, California. The DC-8 satisfied the demanding performance specifications required for this mission, including flight endurance exceeding 10 h, range greater than 9,000 km, payload capacity over 11,000 kg, and capability for global operations with long overwater flight segments.

The DC-8 instrument payload as listed in Table 2 combines the original (ATom-1) payload instruments plus sensors added after the ATom-1 deployment. Given the point-to-point ("racetrack") design of the ATom circuit, the originally proposed payload was comprised of proven instruments that had successfully operated on the DC-8 previously and that had experience with remote flights away from a fixed base of operations. The ATom-1 payload consisted of 22 instruments covering a breadth of measurements including primary and secondary reactive gases [e.g., O_3, volatile organic carbon species (VOCs), oxygenated VOCs (OVOCs), NO_x, NO_y species, HO_x], long-lived gases (e.g., CO_2, CH_4, N_2O, halocarbons, O_2, Ar), aerosol size, number, and composition, spectrally resolved solar radiation, and meteorological parameters. Several species (e.g., O_3, CH_4) were measured by multiple instruments on board. Instrument intercomparisons for O_3 and N_2O (Gonzalez et al. 2021; Hintsa et al. 2021), HCHO (St. Clair et al. 2019), and aerosol sulfate (Froyd et al. 2019) have been published to date; we expect further publications to be forthcoming.

Following ATom-1, an additional five instruments were added to fill in measurement gaps. These instruments provided new measurement capabilities for inorganic halogenated compounds and total aerosol extinction, which were not measured by the original payload, and parallel measurements of NO_2, peroxyacetyl nitrate species (PANs) and SO_2 by different measurement techniques. Also added was analysis of brown carbon on filter samples collected by soluble acidic gases and aerosols (SAGA). The added PAN chemical ionization mass spectrometer (CIMS) instrument provided higher time resolution measurements and speciation of PAN variants; the SO_2 laser-induced fluorescence (LIF) provided the higher precision and sensitivity and lower limits of detection needed for measuring the relatively low SO_2 mixing ratios present in the remote troposphere and stratosphere (Rickly et al. 2021; Rollins et al. 2016); and the NO_2 LIF was added for comparison to the chemiluminescence NO_2 measurements to address concerns of potential interferences at high altitudes that had been noted during a previous aircraft campaign (Nault et al. 2015; Travis et al. 2016).

Flight details. Research flights for the four ATom deployments occurred from 28 July to 22 August 2016 (ATom-1), 26 January to 22 February 2017 (ATom-2), 28 September to 26 October 2017 (ATom-3), and 24 April to 21 May 2018 (ATom-4), lasting ~28 days each (Table ES2). Deployments originated and terminated at the NASA Armstrong Flight Research Center facility in Palmdale, California, following a counterclockwise circuit traveling north to Alaska, south through the Pacific, east across the Southern Ocean, north through the Atlantic, west across the Arctic to Alaska, and south returning to Palmdale.

The flight tracks of the four deployments are shown in Fig. 2, with overnight stops indicated by the yellow markers. The intention was to repeat the same flight pattern on each deployment, but some changes occurred due to airport operations, weather, or new scientific opportunities, e.g., the research flight over Antarctica, added for ATom-3 and -4, which allowed Southern Hemisphere polar observations both during and after the ozone hole season. During ATom-1, the aircraft returned to California from Greenland by flying south through Canada, landing in Minneapolis, and then across the continental United States; for ATom-2, -3, and -4, an additional flight west across the Arctic back to Anchorage was added to complete the full circuit

Table 2. NASA ATom instrument payload (https://espo.nasa.gov/atom/instruments).

Instrument name	Primary measurements	Institution	Mission coverage
Original payload instrumentation			
AMP (Aerosol Microphysical Properties)	Size distributions of dry aerosol particles (size range: 3 to ~4000 nm)	NOAA Chemical Sciences Laboratory	ATom-1–4
AO2 (Airborne Oxygen Instrument)	O_2, CO_2	NCAR	ATom-1–4
ATHOS (Airborne Tropospheric Hydrogen Oxides Sensor)	OH, HO_2, NO, naphthalene	Pennsylvania State University	ATom-1–4
CAFS (CCD Actinic Flux Spectroradiometers)	Actinic flux	NCAR	ATom-1–4
CAPS (Cloud, Aerosol, and Precipitation Spectrometer)	Size distributions of ambient aerosol and cloud particles 0.5–930 μm; detection and classification of sequences inside clouds	University of Vienna	ATom-1–4
CIT-CIMS (Chemical Ionization Mass Spectrometer)	HNO_3, H_2O_2, CH_3OOH, HCN, PAA, PNA, SO_2	California Institute of Technology	ATom-1–4
DLH (Diode Laser Hygrometer)	H_2O	NASA Langley	ATom-1–4
HR-AMS (High-Resolution Time of Flight Aerosol Mass Spectrometer)	Organic aerosol, chloride, nitrate, sulfate, ammonium, PM1 sea salt, bromide, iodide, MSA, perchlorate	University of Colorado	ATom-1–4
ISAF (In Situ Airborne Formaldehyde)	HCHO	NASA Goddard	ATom-1–4
Medusa Whole Air Sampler	O_2, CO_2, argon, CO_2 isotope ratios	NCAR, Scripps Institute of Oceanography	ATom-1–4
MMS (Meteorological Measurement System)	Wind, turbulence, temperature, aircraft position	NASA Ames Research Center	ATom-1–4
NOAA Picarro	CO_2, CH_4, CO	NOAA Global Monitoring Laboratory	ATom-1–4
NO_yO_3 (Nitrogen Oxides and Ozone Chemiluminescence)	NO, NO_2, NO_y, O_3	NOAA Chemical Sciences Laboratory	ATom-1–4
PALMS (Particle Analysis by Laser Mass Spectrometry)	Biomass-burning aerosol, sea salt, mineral dust, sulfate/organic aerosol, and other size-resolved aerosol types	NOAA Chemical Sciences Laboratory	ATom-1–4
PANTHER (PAN and Trace Hydrohalocarbon GC-ECD)	PAN, H_2, CH_4, CO, N_2O, SF_6, CH_3Cl, CH_3Br, CH_3I, OCS, $CFCl_3$, CF_2Cl_2, Halon-12111, CFC-113, HFC-134a, HCFC-141b, HCFC-142b	NOAA Global Monitoring Laboratory	ATom-1–4
PFP (Programmable Flask Package)	N_2O, SF_6, H_2, CS_2, OCS, CO_2, CH_4, CO, CFCs, HCFCs, HFCs, methyl halides, light hydrocarbons	NOAA Global Monitoring Laboratory	ATom-1–4
QCLS (Quantum Cascade Laser System)	CO_2, CO, CH_4, N_2O	Harvard University	ATom-1–4
SAGA (Soluble Acidic Gases and Aerosols)	Na^+, NH_4^+, K^+, Mg^{2+}, Ca^{2+}, Cl^-, Br^-, NO_3^-, SO_4^{2-}, aerosol NO_3^-, aerosol SO_4^{2-}, brown carbon (BrC)	University of New Hampshire, Georgia Institute of Technology (for BrC)	ATom-1–4
SP2 (Single Particle Soot Photometer)	Black carbon (BC), scattering aerosols	NOAA Chemical Sciences Laboratory	ATom-1–4
TOGA (Trace Organic Gas Analyzer GC-MS)	Non-methane hydrocarbons, oxygenated volatile organic compounds, halocarbons, DMS, HCN, CH_3CN	NCAR	ATom-1–4
UCATS (UAS Chromatograph for Atmospheric Trace Species	N_2O, SF_6, CH_4, CO, O_3, H_2, H_2O	NOAA Global Monitoring Laboratory	ATom-1–4
WAS (Whole Air Sampler)	Non-methane hydrocarbons, halocarbons, alkyl nitrates, OCS, DMS	University of California, Irvine	ATom-1–4
Instrumentation added after ATom-1			
GT-CIMS (Chemical Ionization Mass Spectrometer)	PAN, PPN	Georgia Institute of Technology	ATom-2–4
NOAA ToF-CIMS (Time of Flight Chemical Ionization Mass Spectrometer)	HCOOH, $ClNO_2$, N_2O_5, BrO, Cl_2, BrCN, BrCl, $C_2H_4O_3S$	NOAA Chemical Sciences Laboratory	ATom-3–4
SO_2 LIF (Laser-Induced Fluorescence)	SO_2	NOAA Chemical Sciences Laboratory	ATom-4
CANOE (NO_2 LIF)	NO_2	NASA Goddard	ATom-4
SOAP	Aerosol extinction and absorption	NOAA Chemical Sciences Laboratory	ATom-4

and gain more extensive observational coverage in the northern high latitudes as well as in the North Pacific on the final Anchorage to Palmdale flight. Additionally, for ATom-3 and -4, an Antarctic flight was added out of Punta Arenas that extended the latitudinal coverage of the mission to 86°S. Some further variability of the flight tracks occurred due to operational circumstances or weather-related diversions. After ATom-1, the South Pacific stop was moved from American Samoa to Fiji due to runway conditions; the South Atlantic stop on ATom-4 was shifted from Ascension Island to Recife, Brazil, for similar reasons. The Greenland stop proved to be the most problematic, with the intended stopover in Thule occurring only on ATom-2. Kangerlussuaq was used for ATom-1 due to runway repairs in Thule, and weather conditions forced diversions to Bangor, Maine, for ATom-3 and to Kangerlussuaq, followed by a short ferry flight to Bangor, for ATom-4.

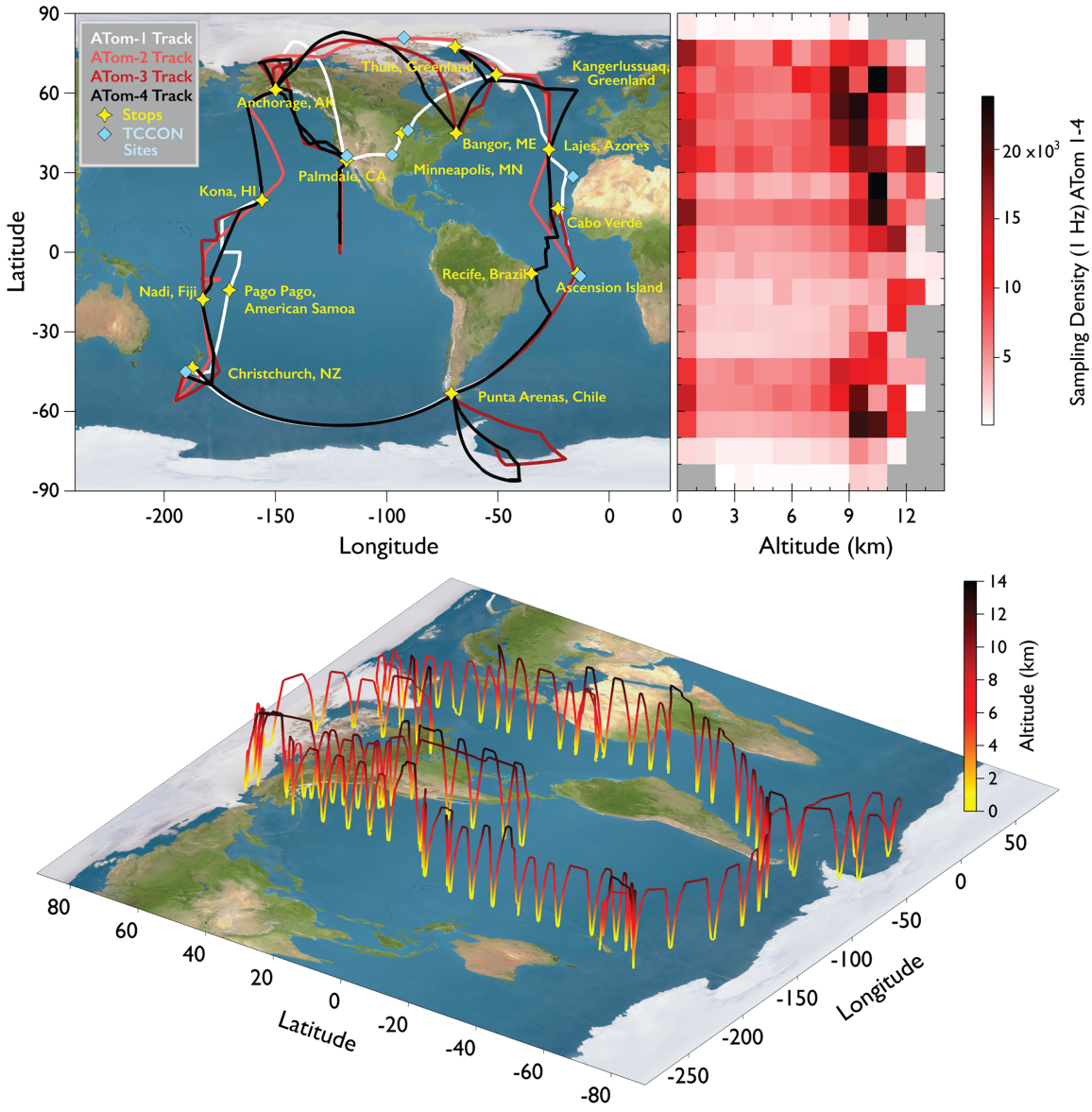

Fig. 2. (top left) Map of the flight tracks and stops for the four ATom deployments. Also noted are the Total Carbon Column Observing Network (TCCON) sites over which ATom performed vertical profiles for measurement intercomparisons. (top right) Density matrix aggregating the entire 1-Hz dataset for ATom-1–4 illustrating the data coverage achieved for the campaign. Data are binned by 10° latitude on the *y* axis and 1-km altitude on the *x* axis and colored by the number of 1-Hz data points in each bin. (bottom) Flight track of ATom-3 shown as an example of the tomographic vertical profiling pattern implemented on the ATom deployments.

Figure 2 illustrates the flight track for ATom-3 along with the spatial sampling statistics for the full mission from 90°N to 90°S latitude and up to 13-km altitude. A total of 645 vertical profiles (including takeoffs and landings) were completed over the four deployments, with a total distance flown of 301,000 km (7.5 times the circumference of the Earth). Statistics for each of the individual flights are provided in Tables ES2 and ES3 and Figs. ES2 and ES3. The low-altitude legs extended into the planetary boundary layer at a nominal altitude of 0.15 km above the ocean surface, and the high-altitude legs extended to an altitude of 11–13 km (depending on fuel load), sufficient to reach the lower stratosphere at high latitudes in both hemispheres. Over the four deployments, 9% of the >400 h of flight time were spent within the boundary layer and 12% were spent in the stratosphere (Table ES3 and Fig. ES2). About 60% of total flight time was spent in profiles (either ascent or descent) and 40% in level flight (high or low altitude). Rates of climb and descent were relatively gradual, averaging +0.4 and −0.5 km min^{-1}, respectively, to provide sufficient sampling time for the instrumentation on board. When possible during the ATom flights, vertical profiles were performed over the TCCON sites noted in Fig. 2 for cross calibration with ground-based remote sensing measurements of total column CO_2, CH_4, CO, and N_2O.

Flight meteorology and forecasting. During each ATom deployment, daily forecast briefings were conducted for each upcoming flight for en route meteorology, chemical composition, and airfield weather conditions. These briefings by a meteorologist and an atmospheric chemist were attended by both in-field scientists and remotely connected university, NOAA, and NASA scientists. These briefings were closely coordinated with the DC-8 mission managers, pilots, aircrew, mission meteorologist, and the mission scientist.

For each DC-8 flight, a mission meteorologist was on board the DC-8 to work closely with the lead mission scientist, DC-8 mission manager, and pilots to help select the specific locations for the vertical profile maneuvers (VPMs)—mainly to avoid thick cloud, weather hazards, and low clouds that obscured the surface. In particular, descents over open ocean to 0.15 km (500 ft) required a visual surface identification by the pilots (VFR; visual flight rules). The ATom "real-time" meteorology was based on a combination of the DC-8 weather radar and forward view camera, plus forecast maps and near-real-time satellite imagery downloads via a satellite communication link to the DC-8 from NASA Langley Research Center.

Flights were monitored remotely by on-ground scientists across the United States using the "Mission Tools Suite" developed by the NASA Ames Research Center in conjunction with a satellite-linked chat with the entire DC-8 team. The on-ground scientists worked closely with the onboard mission meteorologist to assist the real-time aircraft maneuvering and to notify the DC-8 team of changing weather conditions along the route and at the landing site. The mission meteorologist was also tasked with identifying heavy and deep precipitation regions en route, and for in-flight briefings to the instrument scientists on conditions. The pilots tightly coordinated the VPMs between air traffic control, the mission scientists, the mission meteorologist, and the mission manager. Meteorological forecasts were provided by the NASA Goddard Earth Observing System version 5 (GEOS-5) model and the National Centers for Environmental Prediction (NCEP).

A large group of photochemical models helped prepare for ATom flights, supplying chemical forecasts in the field, delivering ATom model data products, or providing multimodel assessments of ATom data (Table 3). This group includes (i) the six global 3D CTMs or CCMs that were represented by science team members and contributed to the pre-ATom methodology papers; (ii) the NASA GEOS-FP model that produced preflight chemical forecasts; (iii) the NASA Goddard Space Flight Center (GSFC) Global Modeling Initiative (GMI) that prepared postflight simulations of chemical reactive species; (iv) the photochemical models calculating the ATom product of parcel reactivities; and (v) an international group of models assessing cloud effects on photolysis rates using ATom data (Hall et al. 2018).

Table 3. Primary models used for ATom forecasting and analysis.

Model name	ATom products
Forecasting/flight planning	
GEOS-FP	GEOS Forward Processing (FP) meteorological products interpolated to the flight tracks: winds, vorticity, humidity, temperature, tracers (e.g., CO, SO_2, black carbon)
NCEP	Preflight meteorological forecasts
Analysis	
CAM4-chem CCM	Pre-ATom chemical climatology, including reactivities, for August (ATom-1) in typical years
GEOS-Chem CTM	Pre-ATom chemical climatology, including reactivities, for August (ATom-1) in typical years
GFDL-AM3 CCM	Pre-ATom chemical climatology, including reactivities, for August (ATom-1) in typical years
GISS-E2 CCM	Pre-ATom chemical climatology, including reactivities, for August (ATom-1) in typical years
UCI CTM	Pre-ATom chemical climatology, including reactivities, for August (ATom-1) in typical years
GMI CTM	GMI full chemistry CTM hindcast of ATom flights with 4D grid bounding each ATom research flight path; gas-phase chemistry along 10-s merge, interpolated to the flight track
TRAJ-3D	3D 30-day back trajectories, convective influence, and boundary layer influence for air parcels sampled along each ATom research flight path

Overview of atmospheric conditions during atom deployments

Meteorological conditions. ATom sampled both Arctic and Antarctic air masses, through the midlatitudes and across the intertropical convergence zones (ITCZ) on each of its four deployments. These flights provided a basic meteorological snapshot of the Earth's remote atmosphere.

The ATom deployments were flown in temperature conditions that were warmer than the MERRA-2 (Modern-Era Retrospective Analysis for Research and Applications, version 2; Gelaro et al. 2017) climatology on average, with occasional below-average regions. The top panel of Fig. 3 shows temperature anomalies over the ATom-1 period (August 2016 average) with respect to the mean conditions over the 1980–2015 time period according to MERRA-2 climatology in the upper troposphere (300 hPa). The 300-hPa level is generally representative of the upper level of the ATom flights. At 300 hPa, global temperatures were 0.7, 0.5, 1.0, and 0.2 K above the 1980–2015 average for ATom-1 to -4, respectively. Surface temperatures (not shown) were 0.5, 0.6, 0.4, and 0.3 K above average. ATom-4 (24 April–21 May 2018) temperatures in the Southern Hemisphere (SH) at 300 hPa (30°–90°S) were 0.3 K below average, a notable exception. All four ATom deployments were flown during a negative phase of the ENSO index (Fig. ES4).

ATom sampling covered all climatic regions of the Earth. Figure 3 displays the position of the ITCZ as purple symbols for the average period of ATom-1. The Fig. 3 surface plot (bottom panel) streamlines (black) show the dominant trade-wind convergence into the tropical region. This surface trace-wind convergence is balanced by divergence at the 300-hPa level (top panel). The jet stream axis (green points in Fig. 3) separates subtropical from midlatitude air. In each ATom deployment, the ITCZ was crossed in both the Pacific and Atlantic, with an added crossing south of California conducted at the start of each ATom deployment. ATom also sampled midlatitude air separated from the subtropics across the subtropical jets in all four seasons.

ATom sampled air from the boundary layer to the stratosphere, as shown in Fig. 4 for ATom-1. The top cross section roughly follows the north–south flight legs down the middle of the Pacific Ocean from Palmdale, California, to Anchorage, Alaska, and south to Punta Arenas, Chile. The bottom cross-section follows the south-to-north path from Punta Arenas, Chile to Kangerlussuaq, Greenland, and on to Minneapolis, Minnesota. Both cross sections highlight the various "regions" sampled: lowermost stratosphere in the extratropics (above the blue line), boundary layer (all latitudes, below the green line), the ITCZ in both the Pacific and Atlantic, the subtropics (equatorward of the jet), midlatitudes, and the polar regions.

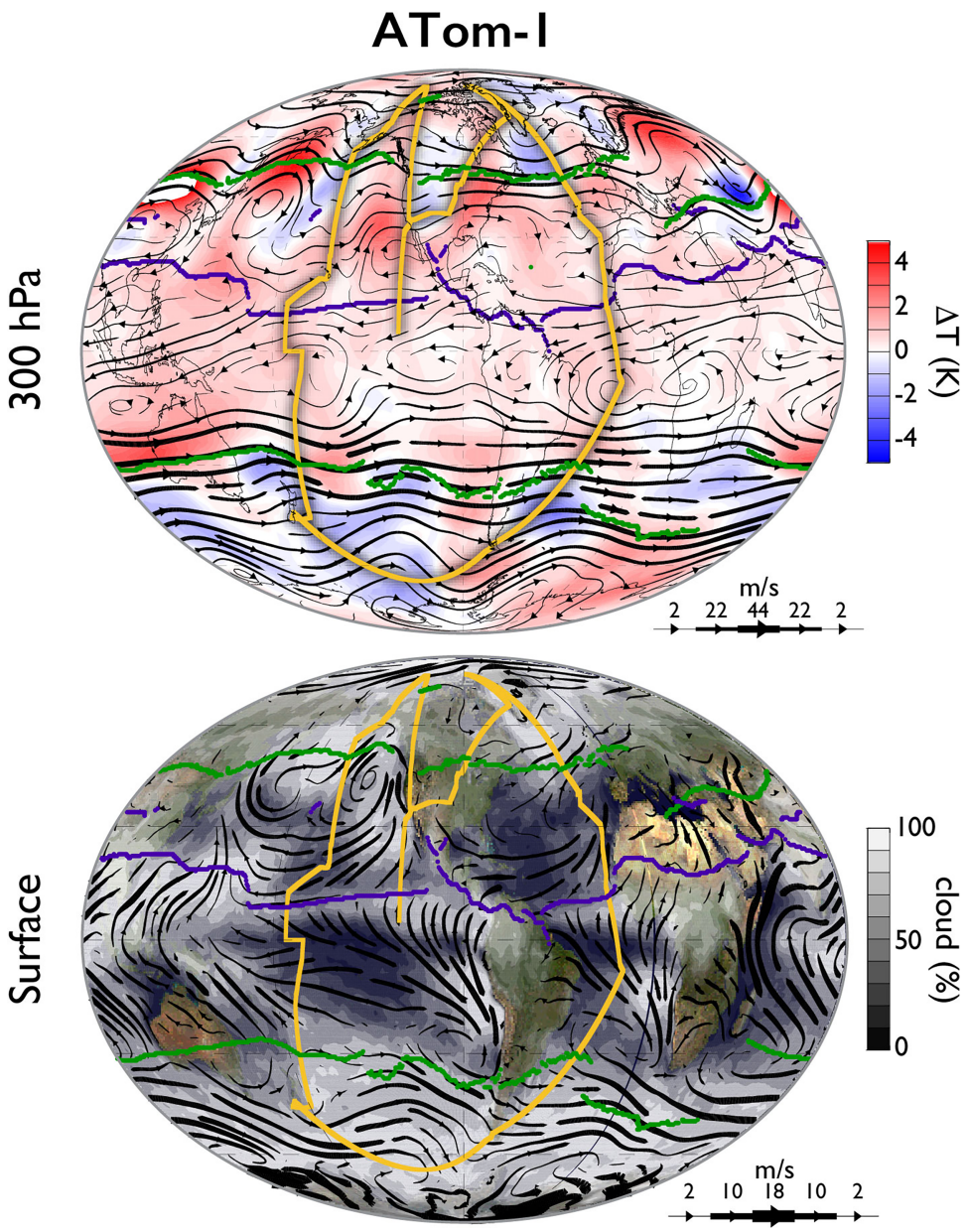

Fig. 3. (top) Temperature deviations (blue-to-red scale) from mean conditions over the 1980–2015 time period according to the MERRA-2 climatology, along with streamlines (black) during ATom-1 (August 2016 average) at 300 hPa. (bottom) Monthly average August 2016 CERES cloud-cover fraction (shading) and MERRA-2 streamlines (black) at surface level. The ATom flight tracks (yellow), the ITCZ (purple), and the jet axes (green) are superimposed on both panels.

The tropics were well sampled during ATom in both the Pacific and Atlantic sectors. In Fig. 3, the ITCZ region was characterized by surface inflow from the subtropics with a deep zone of high relative humidity (not shown). The tropics were also characterized by warm and moist air within 1–2 km of the surface and the associated trade wind cumuli cloud that was capped around 2 km (see Fig. 4 for boundary layer height from MERRA-2). While high RH values are found at the ITCZ up to the tropopause, relatively low RH is found away from the ITCZ in the free troposphere (not shown). The DC-8 altitude ceiling was far below the tropical tropopause, precluding stratospheric observations at these latitudes.

The sampling of the polar stratosphere achieved in both hemispheres during all ATom deployments was limited to only a few kilometers above the tropopause. Nevertheless, some very high levels of ozone, above 0.5 ppm, indicate that this stratospheric air was effectively well above the mixed layer near the tropopause. For the ATom-3 and -4 deployments, an

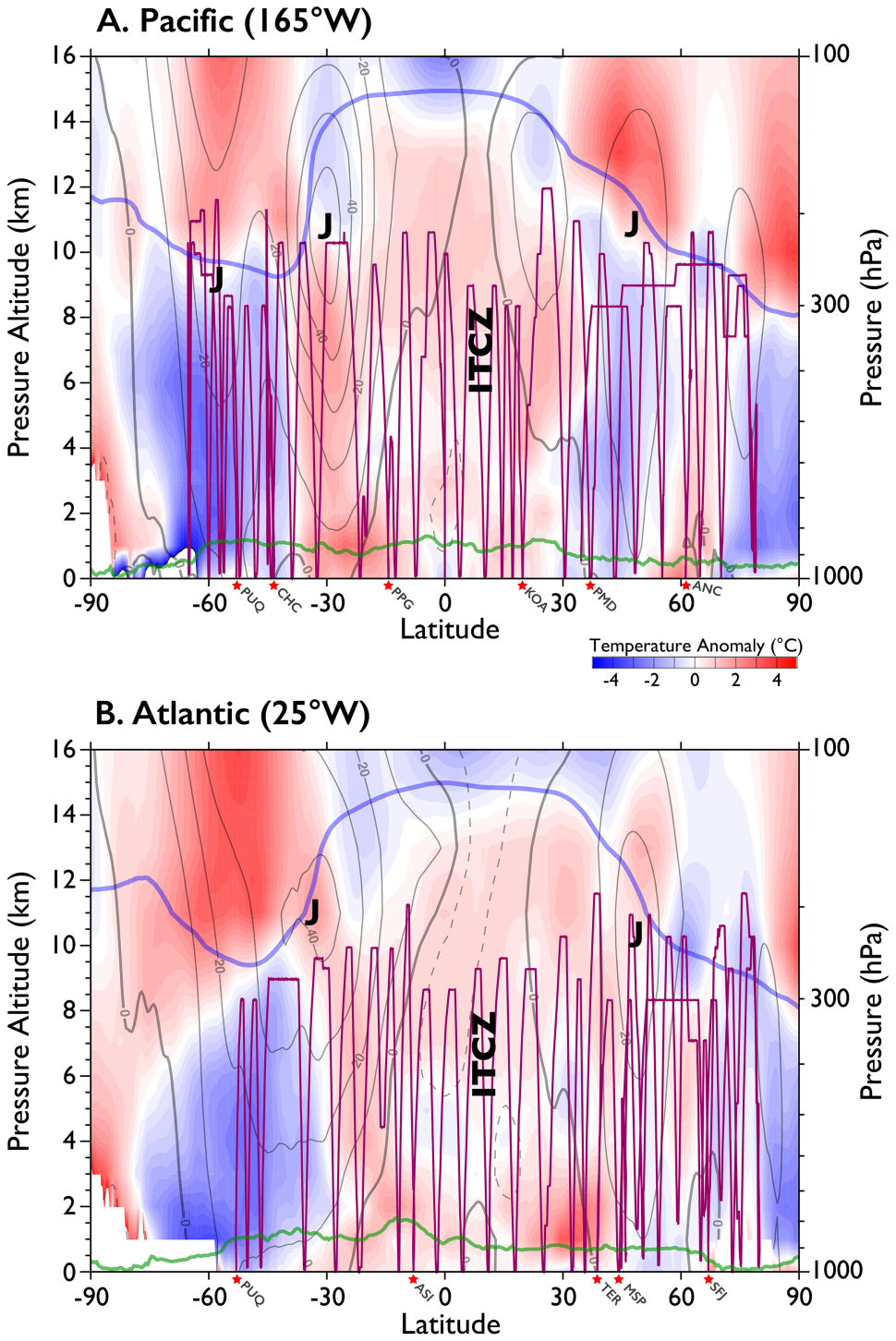

Fig. 4. Temperature anomalies (blue-to-red scale) from a 1980–2015 MERRA-2 climatology, along with zonal mean winds (gray) during ATom-1 (August 2016 average) at (top) 165°W (Pacific sector) and (bottom) 25°W (Atlantic sector). The ATom flight tracks (magenta), the tropopause (blue), and the boundary layer height (green) are superimposed. Airfield latitudes (with three-letter codes) are noted at the red stars at the bottom. The jet locations (J) and ITCZ are also noted.

additional flight was added from Punta Arenas to Antarctica and back. During ATom-3 (October 2017), this flight occurred during the annual stratospheric ozone hole phenomenon. The flight altitude did not reach the most depleted air, but reduced ozone levels were encountered in the lowermost stratosphere.

Occasionally it was necessary to deviate from the design flight track to avoid strong convective clouds or icing conditions. The VFR requirements for the low altitude legs also necessitated that we avoid low-altitude clouds to reach the marine boundary layer (MBL).

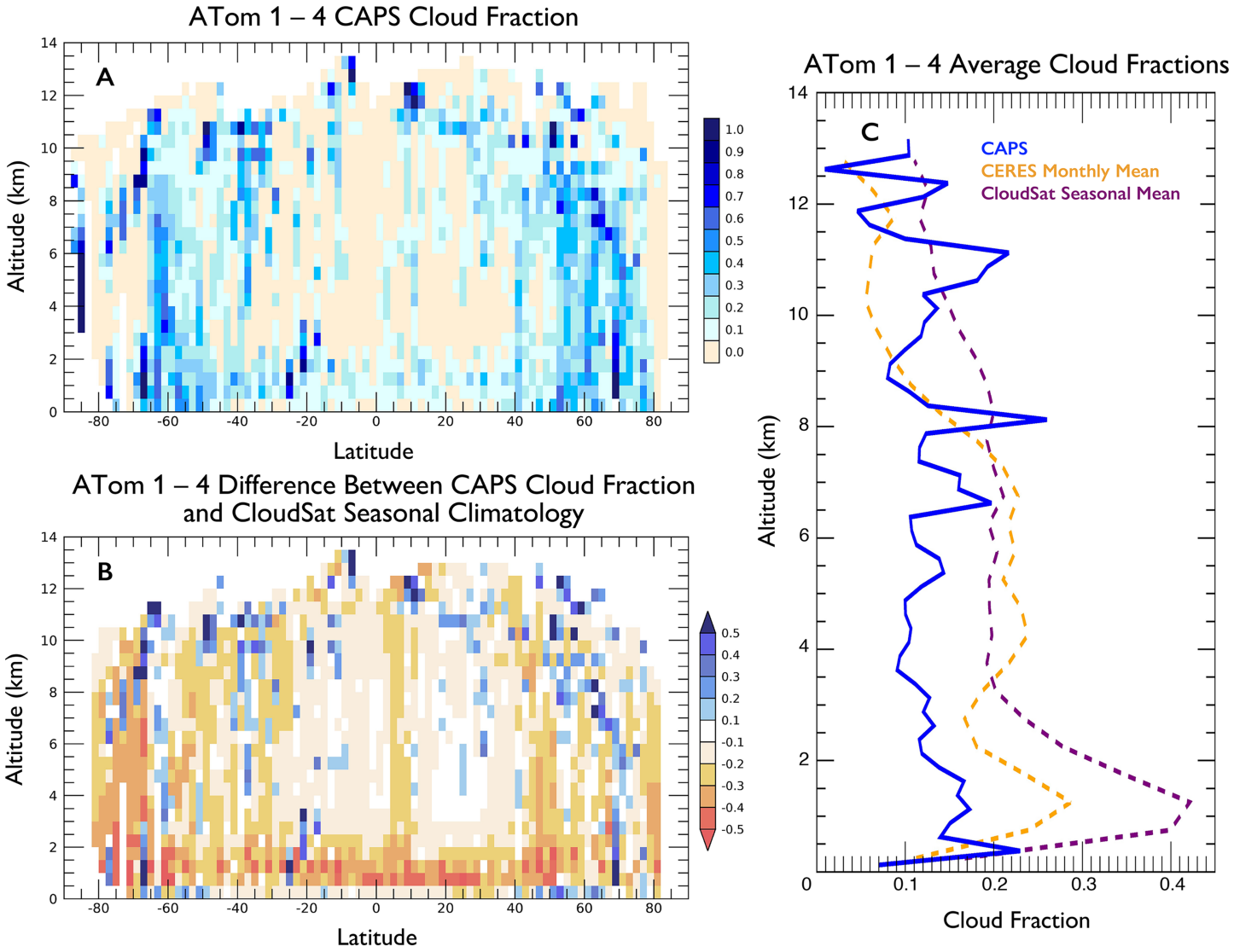

Fig. 5. Summary of in-cloud sampling over the four ATom deployments relative to "typical" cloud climatologies. (a) In-cloud sampling fraction over the four ATom deployments as measured in flight by the underwing-mounted CAPS probe. (b) The difference between the cloud fraction measured by CAPS and the seasonal cloud climatology derived from *CloudSat*. (c) Vertically resolved average cloud fraction measured by CAPS compared to the *CloudSat* seasonal mean and the CERES monthly mean. These figures show that the greatest cloud-free bias during ATom occurred for altitudes below 6 km.

These factors led to an apparent undersampling within clouds. To estimate the degree of in-cloud undersampling, we compared in situ data from the underwing-mounted cloud, aerosol, and precipitation spectrometer (CAPS) probe, which measured and identified cloud types encountered in flight, categorized as liquid, cirrus, or clouds in the mixed-phase temperature regime, to the average cloud climatology for the mission period derived from *CloudSat* and CERES satellite observations. The CAPS identifies the presence of clouds using an algorithm that combines concurrent measurements of particle number concentration, particle size ratios, air temperature, and humidity.

In Fig. 5, we summarize the CAPS observations for the four ATom circuits and the comparison to the satellite climatology. We note that these values represent only an approximation of the potential in-cloud undersampling due to the spatial and temporal differences between the aircraft and satellite observations. Over the four deployments, the CAPS measurements indicated that the DC-8 sampled in clouds between 10.8% and 15.6% of the flight time (average of 12.8%). Of the 53 sampling hours spent in-cloud, 14% were in liquid-phase clouds

and 43% each were in mixed-phase temperature regime and cirrus clouds. The sampling weighted cloud fraction over all locations is 0.129 for CAPS and 0.196 for *CloudSat*, thus, the ATom mission sampled clouds roughly two-thirds as much as would be expected from average climatological conditions if no cloud avoidance maneuvers had occurred. As illustrated by the vertical profile shown in Fig. 5, the most prominent regions of cloud undersampling were below 2 km at all latitudes, in the ITCZ at all altitudes, and in the extratropics generally below 6 km. This result is consistent with expectations given the more frequent cloud avoidance maneuvers that had to be performed at lower altitudes to reach the marine boundary layer. The only regions where ATom sampled significantly more clouds than expected compared to climatology occurred above 6 km, predominantly in cirrus. Importantly, this apparent in-cloud undersampling did not have any consequences on achieving the primary mission goals of ATom; however, we note this condition for the awareness of those who may use the ATom dataset in the future.

Chemical conditions. The representativeness of the ATom sampling periods relative to "typical" chemical background conditions was evaluated for ATom-1 by Strode et al. (2018) using carbon monoxide (CO) and aerosol optical depth (AOD). Overall, the ATom-1 period represented conditions that were relatively cleaner than average, but within the range of climatology for most regions—in the 25th–50th-percentile range of the 2000–16 interannual variability (IAV). The tropical Atlantic region was a notable exception, where ATom-1 data were close to the 75th percentile of the IAV for both CO and AOD. The tropical Atlantic is heavily impacted by biomass-burning emissions from Africa, which are a strong source of both CO and aerosols. Figure ES5 shows global maps of aerosol optical depth and fire locations derived from MODIS for the time periods of the four ATom deployments.

In a separate analysis, Bourgeois et al. (2020) evaluated the chemical representativeness of all four ATom deployments with respect to tropospheric ozone by comparing to long-term ozonesonde records from global monitoring sites, plus extensive higher altitude sampling from the IAGOS project, and previous Pacific transects from the HIPPO campaign. The authors concluded that the ATom missions were consistent with the measurement-based climatologies of tropospheric O_3 and captured 30%–71% of the variability seen in long-term records.

Highlighted outcomes and results

The ATom mission resulted in an extensive and comprehensive global-scale tomographic dataset that includes detailed in situ measurements that had never been made across much of the remote atmosphere and/or had not been measured repeatedly over different seasons. Over 65 peer-reviewed articles using ATom data have been published to date (Table ES4), with many more yet to come. These publications present a wide range of new analyses (e.g., Wolfe et al. 2019) and/or unexpected observations, from a particle of enriched uranium-235 (Murphy et al. 2018) to a new chemical product of marine-emitted sulfur that had never been observed previously in the atmosphere (Veres et al. 2020). These data have also been central in numerous collaborative publications, summarized in Fig. 6, evaluating satellite retrievals of atmospheric traces gases and various chemical and transport models. In the following, we highlight a selection of some significant outcomes published to date.

Global-scale distribution and seasonality of gases and aerosols. Figure 7 presents three-dimensional curtain plots of CH_4, O_3, and BC observations during ATom-3, illustrating the global-scale coverage and fine-grained resolution of the ATom dataset. The distinct north versus south hemispheric gradient in long-lived species, such as methane, is evident, as is the impact of strong pollution sources such as Asian continental outflow and Australian and African biomass burning, as evidenced by both O_3 and BC. The sometimes very distinct

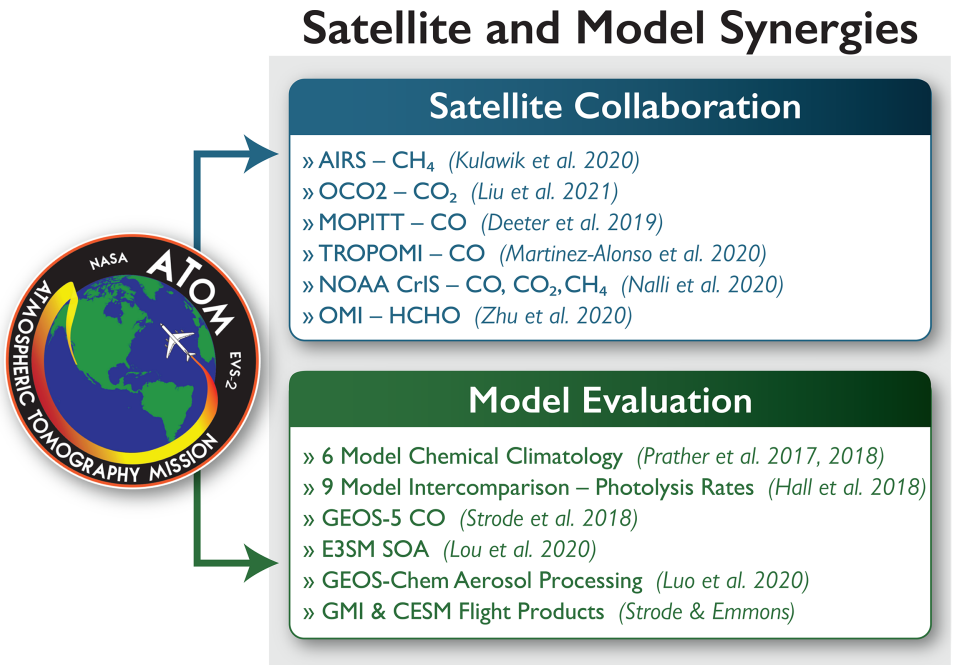

Fig. 6. Summary of analyses and evaluations of satellite data products and model outputs to date using ATom datasets.

differences in composition between the marine boundary layer, the free troposphere, and the lower stratosphere, are also evident, notably for O_3. Similar plots of these three species for all four deployments, illustrating the seasonal differences in distribution and concentration, can be found in Figs. ES6–ES8.

Figure 8 compares and contrasts the probability distributions for three exemplar species in the Pacific and Atlantic Ocean troposphere over four seasons. These plots show both that the distribution profile of individual species can vary markedly with time of year [e.g., unimodal versus bimodal O_3 distributions in the Pacific during ATom-1 (August) versus ATom-2 (February)], and that the distribution of key species can be significantly different between the two ocean basins. The Atlantic is frequently the more polluted. Distributions of CO, for example, are wider in the Atlantic, which altogether lacks the clean "background" peak for CO that is seen in the Pacific.

Publications to date have investigated the global distributions and seasonality of CO (Strode et al. 2018), ozone (Bourgeois et al. 2020), nitrogen oxides, HCHO (Wolfe et al. 2019), HO_x (Brune et al. 2020), O_2 (Stephens et al. 2021), and several different aerosol species, including black carbon (Katich et al. 2018), brown carbon (BrC) (Zeng et al. 2020), sea salt (Murphy et al. 2019), biomass-burning smoke (Schill et al. 2020), inorganic aerosols and aerosol acidity (Hodzic et al. 2020; Nault et al. 2021), iodine (gas phase and aerosol) (Koenig et al. 2020), organic aerosols (Hodzic et al. 2016, 2020), and iron-oxide-like aerosols (FeO_x) (Lamb et al. 2021). The nature of the ATom sampling also provides a unique opportunity to evaluate the performance of both models and satellite retrievals on a global scale. Strode et al. (2018) evaluated the NASA GEOS-5 model, which was used during the missions for preflight chemical forecasting, against global distributions of CO from ATom-1. Observations of CO, CO_2, and CH_4 distributions have also been incorporated into assessments of satellite remote sensing observations from MOPITT (Deeter et al. 2019), TROPOMI (Martínez-Alonso et al. 2020), *OCO-2* (Chevallier et al. 2019; Crowell et al. 2019; Liu et al. 2021), *GOSAT* (Liu et al. 2021; Lu et al. 2021), *Suomi-NPP* (Nalli et al. 2020), OMI (Zhu et al. 2020), and AIRS (Kulawik et al. 2021).

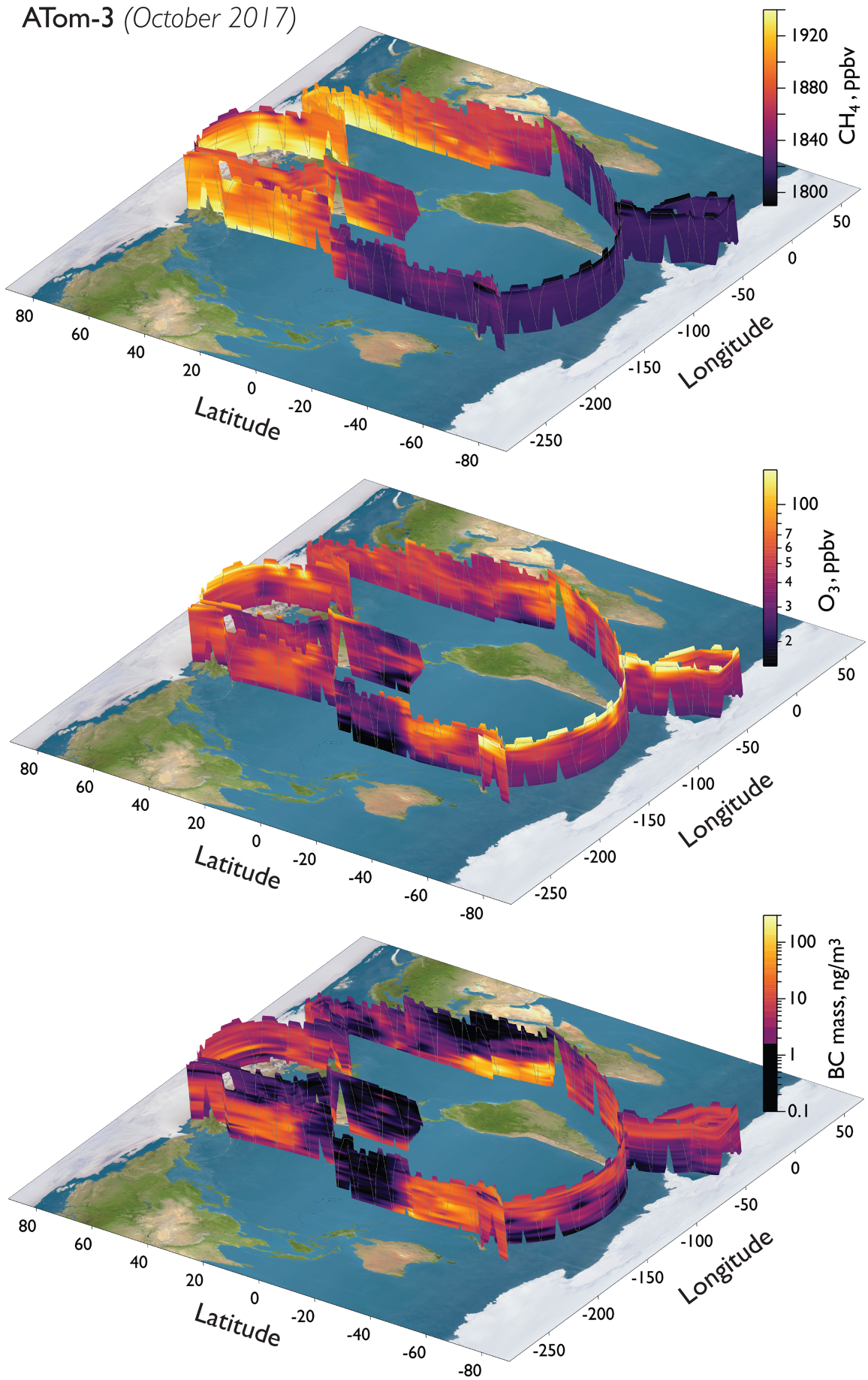

Fig. 7. Example curtain plots showing CH_4, O_3, and BC interpolated from measurements collected along the ATom-3 flight track.

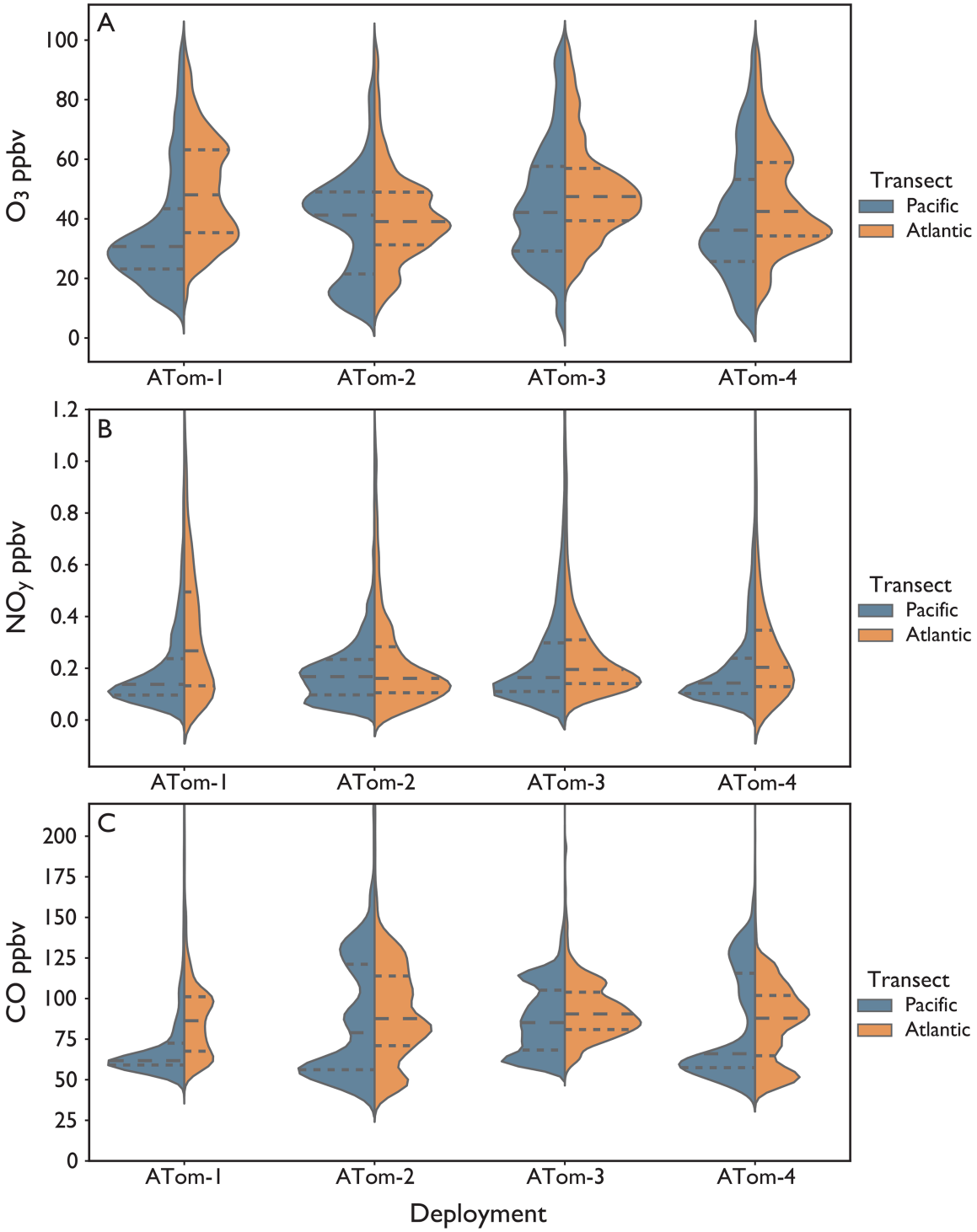

Fig. 8. Probability distributions of tropospheric (top) O_3, (middle) NO_y, and (bottom) CO observed on the Pacific (blue) and Atlantic (orange) transects of the four ATom deployments, which occurred from 28 Jul to 22 Aug 2016 (ATom-1), 26 Jan to 22 Feb 2017 (ATom-2), 28 Sep to 26 Oct 2017 (ATom-3), and 24 Apr to 21 May 2018 (ATom-4). The distributions are normalized to have equal areas under the curves. Dashed lines within each distribution indicate the 25th, 50th, and 75th percentiles of the measurements.

In their analysis of CO, Strode et al. (2018) found that the GEOS-5 model showed considerable skill in predicting the timing and location of plumes, but generally underestimated the magnitude. This was particularly true for strong plumes, which is a known tendency for global models (Eastham and Jacob 2017; Heald et al. 2003). The work by Strode et al. (2018) further investigated the source contributions to CO sampled in ATom-1. They found that

Asian non-biomass-burning sources account for over one-third of the total CO measured in the North Pacific, while both Asian and North American non-biomass-burning make comparable contributions in the North Atlantic. The CO measured in the southern latitudes of both the Pacific and the Atlantic feature a large contribution from oxidation of methane over the remote ocean. All latitudes in the Pacific had a small but persistent contribution of CO from biomass burning from both Eurasia and Africa, while the tropical latitudes in the Atlantic were strongly impacted by African biomass burning.

The far-reaching and wide-ranging impacts of global biomass-burning emissions on the remote atmosphere are a common thread through many of the ATom publications. In addition to CO (Strode et al. 2018) and O_3 (Bourgeois et al. 2020), significant impacts from biomass burning are apparent in the ATom data for NO_y species (e.g., PAN and HNO_3), HCHO (Wolfe et al. 2019), VOCs, methyl halides, organic acids, and several aerosol species, including black and brown carbon.

Katich et al. (2018) compared distributions of black carbon in the Atlantic versus Pacific Oceans, extending the Pacific-only HIPPO observations from Schwarz et al. (2013). They found markedly higher BC loadings in the Atlantic than the Pacific, especially below 4 km off the African coast (see Fig. 7). The authors found that BC's direct radiative effect (DRE) over the whole of the Pacific and Atlantic Oceans is dominated by year-round elevated concentrations of BC at low altitudes over the tropical Atlantic, which is almost exclusively due to long-range transport from fires in Africa. Brown carbon observations reveal a similar story: brown carbon was measured on a global scale for the first time during ATom and was found to be highly heterogeneous and detected primarily in air masses sourced from biomass burning (Zeng et al. 2020). BrC from biomass burning was determined to be an important component of the global radiative balance, with the average DRE due to BrC accounting for ~7%–48% of the total clear-sky instantaneous forcing from carbonaceous aerosols. Moreover, whereas global aerosol models have previously shown a persistent positive bias in overestimating BC in the remote Pacific and at high altitudes (Schwarz et al. 2013), the Katich et al. (2018) study showed that the African biomass-burning outflow changes the direction of the model BC bias with models underestimating the BC loadings in the Atlantic.

In considering total biomass-burning-sourced aerosol, Schill et al. (2020) observed that aged smoke particles are dilute but ubiquitous across the remote troposphere, accounting for an average of more than 27% of the total accumulation-mode aerosol number and 6%–30% of the total aerosol mass across all altitudes in the tropospheric column. Further, biomass-burning smoke tracers were found to be present in over two-thirds of the air masses encountered on ATom, including at altitudes up to 12 km, indicating efficient vertical transport. Indeed, a separate analysis by Murphy et al. (2021) of stratospheric aerosol composition also reported the apparent influence of biomass-burning aerosol injections into the lower stratosphere. Both papers also support the conclusion of Katich et al. (2018) and Zeng et al. (2020) of a significant and widespread contribution of biomass-burning aerosol to global radiative forcing.

Aerosol properties and processes. Aerosol interactions with clouds and radiation remain the largest source of uncertainty in climate models. The radiative forcing effects of aerosols and their impact on gas-phase chemistry are determined by their size, composition, and altitude (Murphy et al. 2021; Watson-Parris et al. 2019). The ATom payload included measurements of aerosol size distribution, chemical composition, and optical properties that, in combination, have already produced valuable new insights and analyses on aerosol properties and processes in the remote atmosphere and have helped to constrain aerosol removal and gas-phase chemistry impacts in models.

Principal aerosol sources and size-resolved composition for different tropospheric environments are revealed by combining particle analysis by laser mass spectrometry (PALMS)

single-particle and high-resolution time of flight aerosol mass spectrometer (HR-AMS) bulk composition with CAPS and AMP particle size measurements (Brock et al. 2021; Froyd et al. 2019; Hodzic et al. 2020), as shown in Fig. 9 for the Pacific Ocean basin during ATom-1 and -2. These observations represent the first global-scale measurements of organic aerosols (OA)

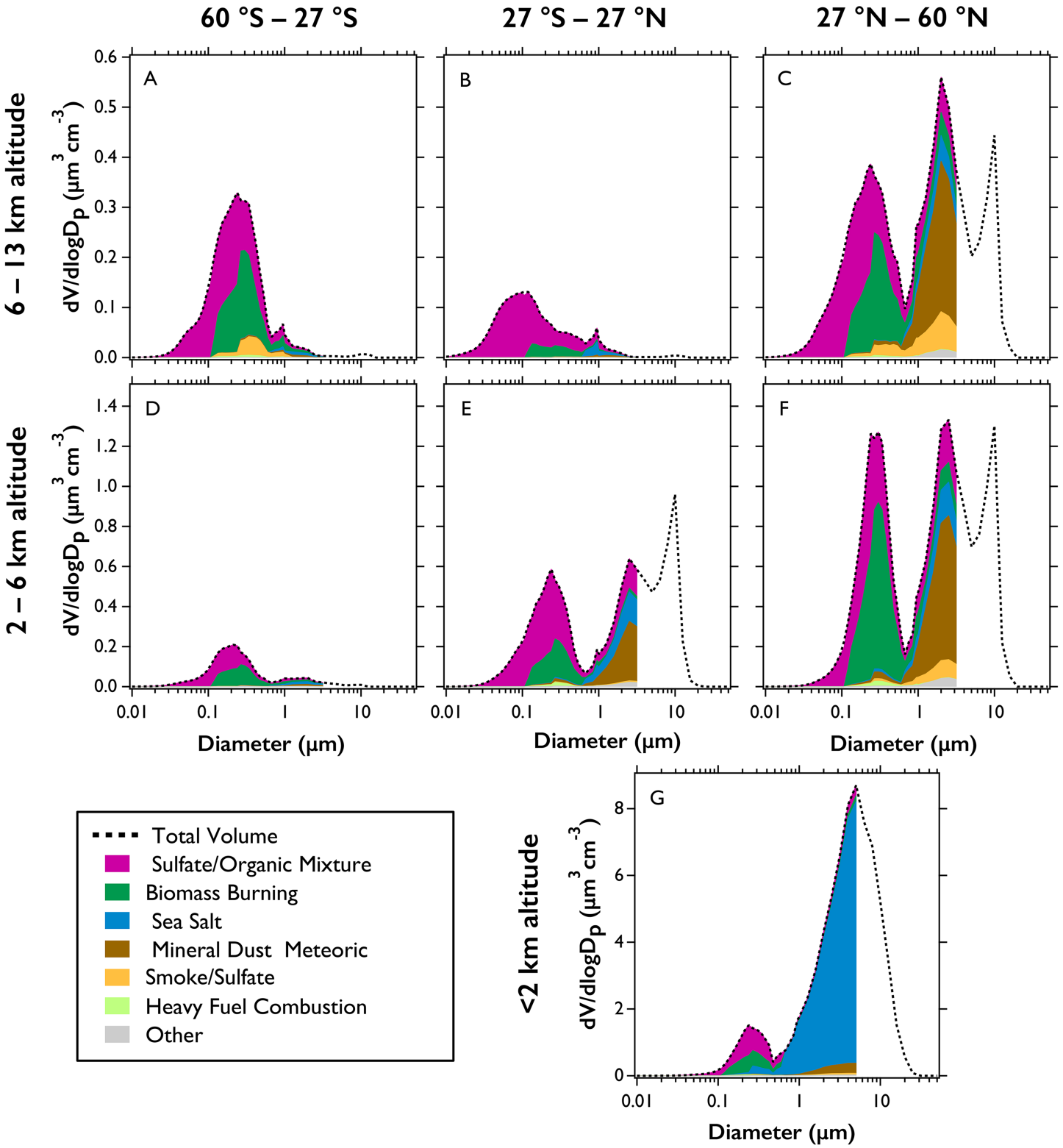

Fig. 9. Average dry aerosol size distributions and composition observed in ATom-1 and ATom-2 over the Pacific Ocean derived using measurements compiled from the AMP, CAPS, HR-AMS, and PALMS instruments. Data are broadly binned by altitude and latitude. Note the differing *y*-axis scales for the three altitude ranges, due to the greater total aerosol volume at lower altitudes. The marine boundary layer data (<2-km altitude) are not binned by latitude since, although the accumulation mode varied in intensity, the composition was found to be similar across latitudes and dominated by sea salt.

and of primary aerosols from sea salt, mineral dust, and smoke. For the cloud condensation nuclei (CCN) size range in the remote troposphere (100–500 nm; Brock et al. 2019) ATom showed that OA was nearly ubiquitous, and a major fraction of the remote aerosol, mostly of secondary origin and highly aged (Hodzic et al. 2020). A detailed comparison with state-of-the-art current CCMs by the same authors showed that while model skill has improved over time, this improvement is partially due to cancelling errors in both the source and loss terms (Hodzic et al. 2016, 2020; Lou et al. 2020). The inorganic fraction of very remote CCN, on the other hand, was highly acidic (typically pH < 0) and consisted mostly of sulfate, with important implications for the particle phase state, hygroscopicity, radiative and chemical properties and, by implication, for the representation of ammonia source in CCMs (Nault et al. 2021).

Mineral dust and sea salt dominate the coarse mode aerosol (Fig. 9), with sea salt displaying a very strong vertical gradient, varying up to four orders of magnitude from the MBL to the upper troposphere (UT) (Bian et al. 2019; Murphy et al. 2019). Above the MBL, very low sea salt concentrations strictly limit the possible contribution of sea salt aerosol to gas-phase halogen abundances and nitric acid in the UT. Unlike sea salt, mineral dust is present at significant levels above the MBL and is a large component of the coarse-mode aerosol in the free troposphere. A forthcoming study will further investigate the global abundance of mineral dust and its potential to seed cirrus clouds.

The tropical UT was found to have consistently low aerosol mass (Fig. 9) and low number concentration of aerosols greater than 60-nm diameter with respect to lower altitudes in this region (Fig. 10a), due in part to efficient aerosol scavenging by clouds and precipitation. Multiple global aerosol models severely overpredict this primary aerosol mass (including BC, biomass-burning aerosols, sea salt, and dust) in the UT (Schwarz et al. 2013; Yu et al. 2019). ATom measurements have already led to major revisions in the convection and wet-scavenging parameterization in the Community Earth System Model's (CESM) Community Aerosol and Radiation Model for Atmospheres (CARMA) and the GEOS/GOCART model, lowering the simulated abundances of climate-relevant aerosols in the UT by orders of magnitude (Bian et al. 2019; Hodzic et al. 2020; Luo et al. 2020; Schill et al. 2020; Yu et al. 2019).

The aerosol size range observed on ATom provided novel insights into new particle formation (NPF). Concentrations of ultrafine particles (diameters of 3–7 nm, Fig. 10b) are elevated in the UT, in contrast to the very low concentrations of larger diameter particles (Fig. 10a). This remarkable result indicates extensive NPF in the tropical UT (Williamson et al. 2019). Earlier studies previously observed this phenomenon and demonstrated how UT NPF contributes to CCN in the remote lower troposphere of the Pacific (Clarke and Kapustin 2010; Clarke 1993; Clarke and Kapustin 2002). ATom observations reveal that NPF formation persists seasonally at all sampled longitudes over both ocean basins, demonstrating the production of CCN due to condensational growth during gradual descent within the tropics, and characterizing its impact on the Earth's radiation balance. The results indicate that the tropical UT seeds CCN to much of the tropical troposphere.

A highlight of the ATom dataset is the combination of chemical, physical, and optical aerosol measurements that can be used to develop global-scale, vertically resolved, climate-relevant aerosol properties in remote regions and to determine the contributions to aerosol optical depth (AOD) from different aerosol types in different air masses (Brock et al. 2021). This derived dataset offers unique tests of global models and evaluation of assumptions used in retrievals of aerosol properties from both ground-based and satellite remote sensing. While AOD is a valuable satellite product, reducing the uncertainty in aerosol cloud and radiation interactions requires information on the chemical and microphysical aerosol properties, which cannot currently be derived from satellite observations alone.

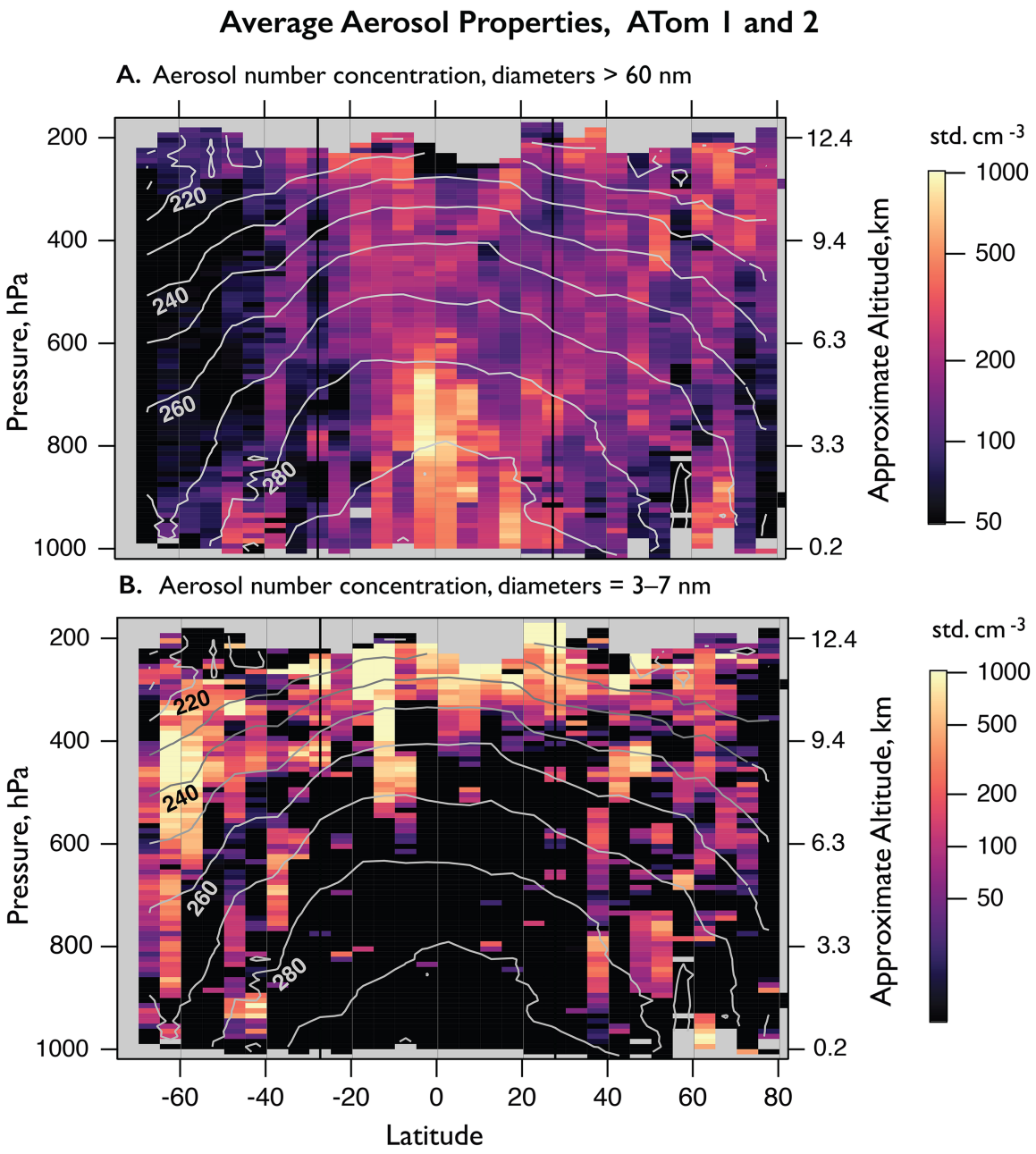

Fig. 10. Curtain plots of aerosol number concentrations (per cubic centimeter at standard temperature and pressure, 273 K and 1 atm), averaged over ATom-1 and ATom-2 and both the Pacific and Atlantic Ocean transects, adapted from data presented in Williamson et al. (2019). The number concentrations are shown for (a) particles with diameters larger than 60 nm, representing accumulation + coarse mode aerosols that can act as cloud condensation nuclei, and (b) particles with diameters of between 3 and 7 nm, revealing a large source of new particles at high altitudes in the tropics.

Photochemistry and oxidation in the remote atmosphere. A primary objective of the ATom mission is to characterize the photochemical regime in the remote troposphere across four seasons as represented by three major reactivities: photochemical production of O_3 (P-O_3), loss of O_3 (L-O_3), and loss of methane (L-CH_4). These reactivities have been calculated for ATom-1 for each 10-s parcel along the flight tracks using five 3D models and one 0D box model. The models adopt a modeling data stream (MDS) of continuous 10-s species abundances derived from the measured values using interpolation or ATom statistical distributions to fill gaps (Guo et al. 2021). For the 3D models, the MDS data are used to initialize the chemical species, water vapor, and temperature in a grid cell close to where the measurement is made, using observed temperature, pressure, and water vapor. The model then integrates

over 24 h without transport, mixing, scavenging, or emissions (see the A-run of Prather et al. 2017), using the cloud fields normally used in the model for that day. The instantaneous photolysis rates (J values) measured during ATom record the instantaneous cloud effects, but not the history seen by the parcel over 24 h. The box model scales the measured J value over 24 h, but we ask the global models to use five separated days in the month of the deployment to average over differing synoptic conditions. For most of the 3D models used in ATom, the computed reactivities are similar for similar initial chemical composition (see Prather et al. 2018). We show results from the NASA GMI model as an example in Fig. 11. All MDS parcels are weighted to ensure representation by latitude and mass where coverage is adequate. For plotting here, the reactivities of each 10-s parcel are averaged in 1° latitude bins from 30°S to 30°N and 200-m altitude bins from 0 to 12 km.

For the full ATom-1 circuit it was found that air parcels with the highest reactivity (top 10%) account for 25%–30% of the total reactivity. In general, the greatest net O_3 tendency was in the upper troposphere where NO_x was enhanced, though enhanced O_3 production rates were also determined for lower altitudes across the Pacific. The largest rates for L-O_3 and L-CH_4 were found in the lower troposphere associated with warm temperatures and high humidity.

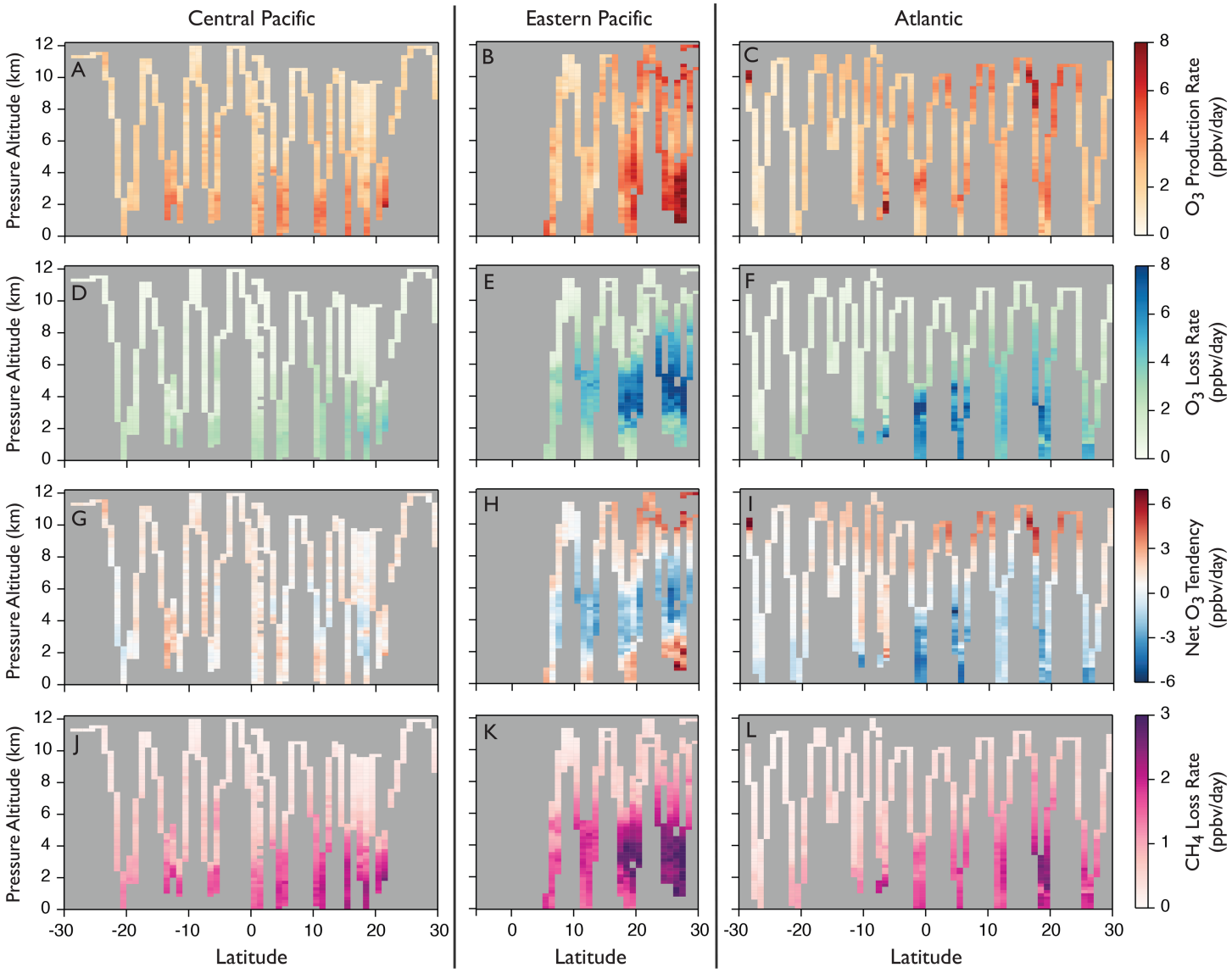

Fig. 11. Rates of photochemical ozone production, ozone loss, net O_3 tendency, and methane loss calculated with the NASA GMI chemical model using measurements collected during ATom-1. Shown are transects in the central Pacific, eastern Pacific, and Atlantic Oceans within the latitude range 30°S–30°N, representing the tropics and subtropics.

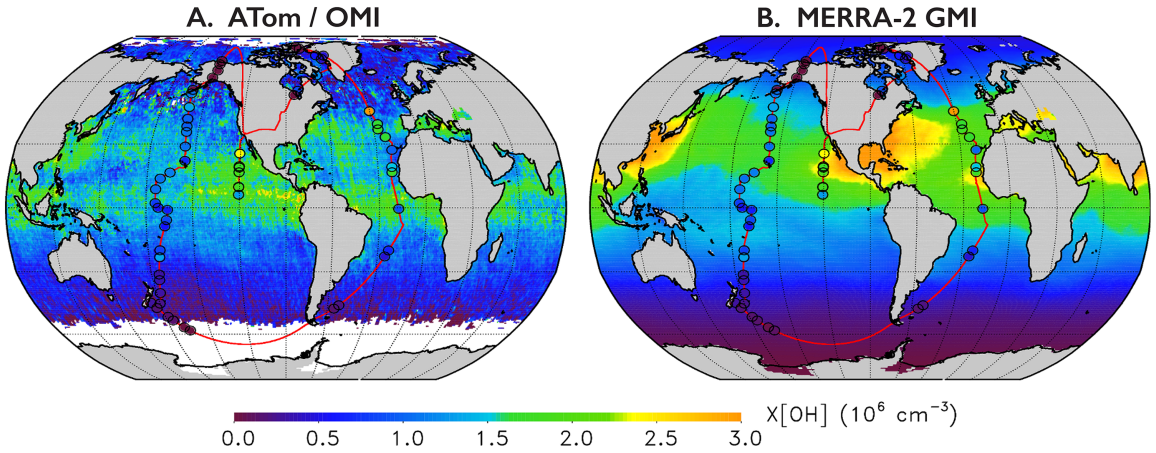

Fig. 12. Diel-average tropospheric column mean OH concentrations (X[OH]) are shown for the ATom-1 deployment period. (a) Global over-ocean values derived from OMI HCHO and ATom observations; (right) Values from the MERRA-2 GMI model simulation. Flight tracks for the ATom-1 deployment are indicated by red lines. Overlaid circles depict in situ OH columns measured by the ATHOS instrument during ATom-1, integrated for individual vertical profiles and scaled to diel-average representative values using hourly output from the MERRA-2 GMI simulation.

Extensive measurements of OH and HO_2 over four seasons allow for a detailed evaluation of photochemical models. Several publications have analyzed the instantaneous measurements from ATom to extend HO_x observations throughout the remote oceanic free troposphere (Brune et al. 2020; Thames et al. 2020; Wolfe et al. 2019). Observed median OH and HO_2 generally agreed with model values within combined uncertainties (±40%), with smaller errors (±20%) below 6-km altitude in some areas. However, OH observations systematically exceeded modeled values at altitudes above 8 km (by ≤35%), pointing to a persistent bias in the free and upper troposphere for the measurements, the model, or both. The extremely low concentrations of key species, such as NO, at high altitudes continues to be a challenge for our current instruments to measure accurately enough to reduce the uncertainty in derived OH.

Wolfe et al. (2019) used the in situ HCHO and HO_x observations from ATom to demonstrate the tightly coupled relationship between remote tropospheric OH and the production and loss of HCHO. Using the observed HCHO–HO_x relationship, satellite-based HCHO retrievals from the Ozone Monitoring Instrument (OMI), and model-derived HCHO loss frequencies, the authors derived global maps of total-column OH abundance throughout the remote troposphere for the ATom-1 (Fig. 12) and ATom-2 time periods. The resultant maps reveal unique features in global OH distribution and seasonality, such as a tenfold-lower concentration of OH in the tropical west Pacific relative to the surrounding area and enhancements in the east Pacific and South Atlantic. This novel analysis leverages ATom data linked to OMI observations to constrain global oxidizing capacity with satellite products.

ATom directly measured OH reactivity along with HO_x. The measurements in the marine boundary layer (Thames et al. 2020) found notably large discrepancies between measured OH reactivity and calculations based on the sum of individual species that react with OH. This "missing OH reactivity" typically ranges from 0% to 50% of the measured OH reactivity, suggesting that there are unmeasured chemical species in some of these environments (Di Carlo et al. 2004; Yang et al. 2016). When averaged over all latitudes and ATom deployments, the measured OH reactivity was 1.9 s^{-1} (±0.64 s^{-1}), which is 0.5 s^{-1} (30%) larger than calculated OH reactivity. Missing OH reactivity in the MBL during flights was often much larger, between 1 and 3.5 s^{-1}, especially in the North Pacific. Correlations between missing OH reactivity and measured HCHO, dimethyl sulfide (DMS), butanal, and sea surface temperature suggest the existence of unmeasured or unknown VOCs or oxygenated VOCs associated with ocean emissions. This missing OH reactivity appears to be inconsistent with OH from a global model

(Travis et al. 2020) if it is due to an alkane, but could be due to, for example, an alkene that recycles OH during subsequent oxidation chemistry.

Marine emissions and air–sea exchange. ATom observed the widespread impact of marine emissions and air–sea exchange on many aspects of the atmosphere, including reactive gases and aerosols, oxidation chemistry, ozone destruction, and cloud formation. Repeated descents into the MBL and periodic three-level stacked flux divergence runs provided a unique and extensive dataset for investigating air–sea exchange across a range of latitudes, seasons, and oceanic biogeochemical regimes. These data provide evidence for marine emissions of oxygenated VOCs, alkyl nitrates, and halogen- and sulfur-containing species, particularly in the tropical and subtropical Pacific. Figure 13 summarizes the ocean-sourced species and related atmospheric processes that have been the subjects of ATom publications to date. These publications collectively show significant and widespread impacts of marine emissions from the remote oceans on tropospheric chemistry and on aerosol and cloud processes, highlighting the importance of incorporating these emissions into global chemistry and climate models.

The world's oceans represent one of the largest organic carbon reservoirs on the Earth and the dissolved organic matter within the sea surface microlayer is known to produce a variety of low-molecular-weight VOCs and OVOCs. The photolysis of OVOCs, in particular, directly impacts atmospheric oxidation as an additional source of HO_x radicals. Analyses of marine

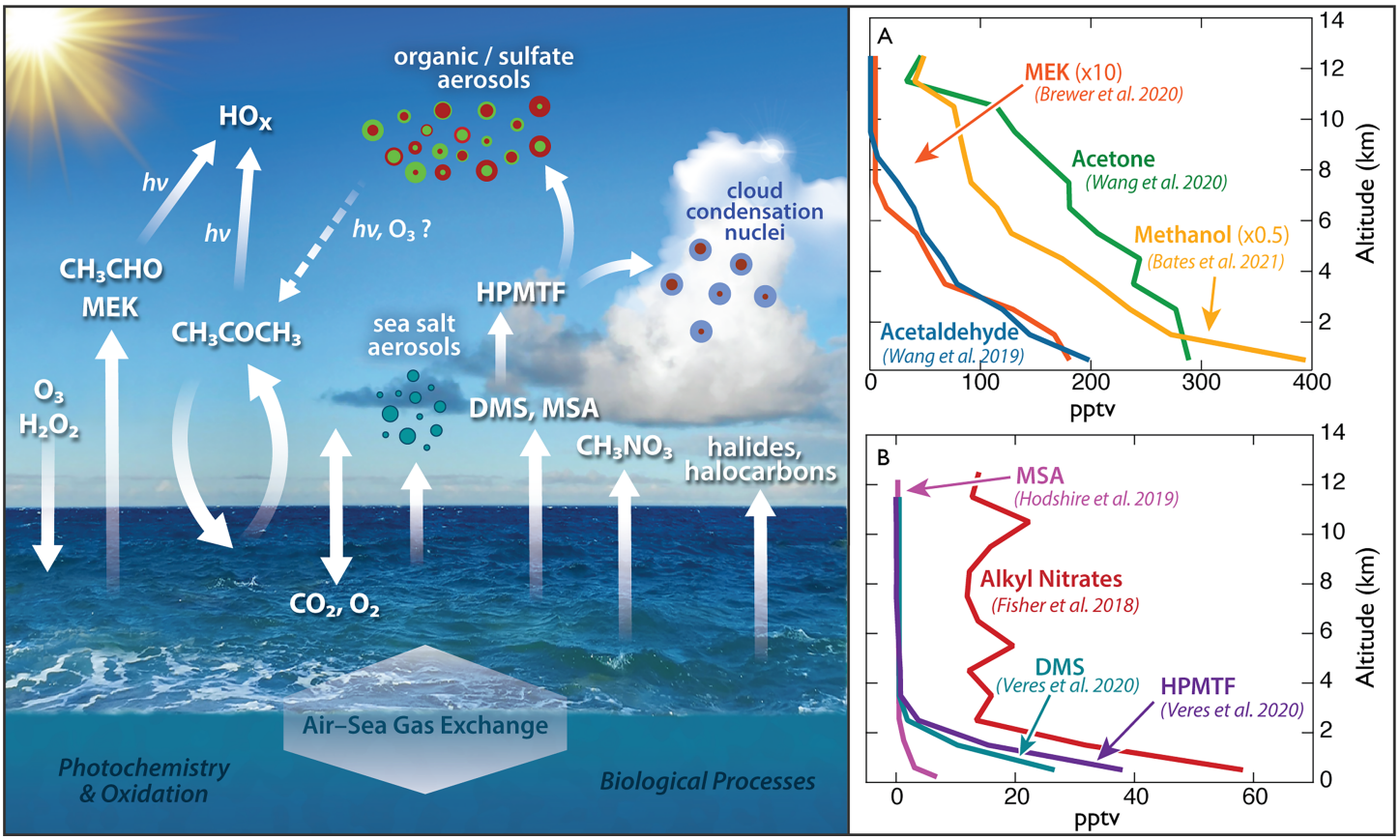

Fig. 13. (left) Schematic illustration summarizing the gases and aerosols with marine sources and/or sinks that have been studied to date using ATom observations. (right) Example vertical profiles of several of these ocean-emitted species, demonstrating the low-altitude enhancements that were observed. All of the vertical profiles represent the median values measured in the equatorial Pacific, from 10°S to 10°N, in 1-km GPS altitude bins. Acetaldehyde, MEK, acetone, methanol, and alkyl nitrates are from ATom-1 and ATom-2 observations; HPMTF is from ATom-3 and ATom-4 observations; DMS is from all four ATom deployments. Alkyl nitrates are the sum of C_1–C_6 alkyl nitrates, of which methyl nitrate is the dominant species.

OVOC emissions from ATom have to date focused on acetaldehyde (Wang et al. 2019), acetone (Wang et al. 2020), methyl ethyl ketone (MEK) (Brewer et al. 2020), and methanol (Bates et al. 2021). Vertical profiles for these VOCs (Fig. 13) show strong vertical gradients from the ocean surface. Concurrent observations of peroxyacetic acid (PAA, not shown), a product of CH_3CHO oxidation, demonstrate a similar MBL enhancement.

Using an observationally constrained box model, Wang et al. (2019) showed that the observed CH_3CHO can explain the observed PAA, providing support for the veracity of both measurements. Standard 3D model simulations, for example the Community Atmosphere Model with Chemistry (CAM-chem; Wang et al. 2019) and GEOS-Chem (Travis et al. 2020), severely underpredict CH_3CHO in the remote global troposphere. The addition of both an oceanic flux parameterization for CH_3CHO and a potential source of CH_3CHO from organic aerosols considerably improved the agreement between the model results (Travis et al. 2020; Wang et al. 2019) and observations.

Emission and air–sea exchange of ketone species, specifically MEK and acetone, were investigated by Brewer et al. (2020) and Wang et al. (2020), respectively. These species have a sufficiently long lifetime to be transported to the free and upper troposphere, where they can serve as an additional source of hydroxyl radicals through photolysis.

The oceans can act as either a source or a sink for acetone. Previous studies have found that the global oceans play a key role in regulating atmospheric abundances of acetone and that oceanic fluxes of acetone can vary significantly in both direction and magnitude with season and latitude. Wang et al. (2020) used ATom-1 and ATom-2 acetone observations (representing Northern Hemisphere summer and winter) to develop a bidirectional oceanic acetone flux parameterization, which was incorporated into the CAM-chem global model. Results from this work show that the tropical and subtropical oceans are mostly a net source for acetone, while the high-latitude oceans are a net sink. Photochemical destruction of acetone was found to be an important source of hydroxyl radical production in the atmosphere, with the largest contribution to total HO_x production (30%–40%) occurring in the tropical upper troposphere.

The world's oceans are also a major source of sulfur compounds to the atmosphere. Dimethyl sulfide (DMS), in particular, has been the subject of a decades-long research effort due to its role as the major natural source of global atmospheric sulfur (Andreae et al. 1985; Bates et al. 1992; Charlson et al. 1987; Quinn and Bates 2011). DMS oxidation across the world's ocean basins produces methanesulfonic acid (MSA) and sulfate aerosol, which in turn affects Earth's albedo and climate, and thus, details of the DMS oxidation mechanism are critical in defining this atmospheric chemistry–climate interaction. Prior to ATom, DMS oxidation chemistry was thought to be generally well understood (Hoffmann et al. 2016). During the ATom mission, a previously obscure molecule, hydroperoxymethyl thioformate (HPMTF, $C_2H_4O_3S$), was observed for the first time in the atmosphere (Veres et al. 2020) and shown to be a major intermediate species in the DMS oxidation pathway at low NO_x concentrations. This unanticipated discovery confirmed a mechanism that had only previously been theorized (Wu et al. 2015). ATom identification of the role of HPMTF represents a significant advance in the understanding of the DMS oxidation mechanism in the MBL.

Summary and outlook

The NASA ATom Mission has provided an extensive and comprehensive atmospheric dataset that has, to date, resulted in over 65 publications addressing wide ranging topics, including oxidation chemistry, aerosol formation and properties, tropospheric and stratospheric composition, radiative forcing of pollutants, aerosol–cloud interactions, and emissions sources of global importance. The mission met its core scientific objectives by employing a comprehensive, tomographic global-scale sampling strategy of atmospheric chemistry and composition unique for airborne field campaigns (Table 1). ATom did not seek out particular

emissions sources or airmass types, opting instead to fly a repeatable pattern to capture an unbiased, statistically significant snapshot of the present-day atmosphere. By not limiting the project to a strict set of predefined targets, ATom became greater than envisioned—a voyage of discovery that has resulted in numerous unexpected and highly significant findings, only a small part of which have been presented here.

The ATom Mission also serves as a powerful example of the continued value of field campaigns with heavy-lift long-range aircraft for advancing atmospheric sciences and our Earth observation capabilities. Airborne platforms fill a critical gap between ground stations and satellite-based remote sensing observations, efficiently sampling over large spatial scales with detailed, vertically resolved measurements at much higher temporal and spatial resolution than can be achieved by global models or satellites. The ATom sampling strategy provides the observations needed to rigorously test satellite retrievals, especially valuable as benchmark datasets to determine retrieval biases that often cannot be quantified any other way. Aircraft observations spanning the globe will become increasingly important as the next-generation of atmospheric composition satellites become operational. In addition, coordinated balloon-borne measurements concurrent with future ATom-style research aircraft flights would be valuable for extending such observations to higher altitudes in the stratosphere that are beyond the reach of the DC-8.

We see exceptional value in tomographic global-scale observations that revisit the global atmosphere periodically in the future. The continued increase in the sophistication of global CCMs and CTMs creates a parallel need for more comprehensive atmospheric measurements of trace gas concentrations and aerosol properties. These models need to be confronted with data having the widest possible geographic, vertical, and seasonal coverages. ATom observations and their interpretation provide a valuable snapshot of the atmospheric state that comes at a critical time when the Earth system is undergoing rapid change. Revisiting the global atmosphere with new observations is an important and critical part of how we can track, quantify, and assess the changing atmosphere, addressing the key questions for Earth science now and in the future.

Acknowledgments. This work is a contribution to the ATom project, an EVS-2 Investigation awarded under NASA Research Announcement (NRA) NNH13ZDA001N-EVS2, Research Opportunities in Space and Earth Science (ROSES-2013) and funded through NASA Agreement NNH15AB12I to NOAA. The National Center for Atmospheric Research is a major facility sponsored by the National Science Foundation under Cooperative Agreement 1852977. The AO2 and Medusa measurements were supported by NSF Awards AGS-1547626, AGS-1547797, AGS-1623745, and AGS-1623748. We acknowledge the many scientists and engineers on the ATom Science Team who contributed their talent, time, and expertise to this mission. We also gratefully acknowledge the NASA and ESPO project managers, site managers, shipping coordinators, mission managers, pilots, aircrew, and ground crew that were essential for the success of this extraordinarily challenging campaign. A full list of the ATom team members can be found in Table ES5 in the online supplemental material. We thank Dennis Dickerson (Respond Grafiks, Broomfield, Colorado) for creating a digital rendering of the NASA DC-8 that was used in Fig. 1 of this article. We thank the many service and hospitality workers in Palmdale, Anchorage, Kona, Pago Pago, Nadi, Christchurch, Punta Arenas, Recife, Ascension Island, Cabo Verde, Lajes, Kangerlussuaq, Thule, Bangor, and Minneapolis who welcomed a large group of tired scientists and crew with warm beds, good food, heroic patience, and flexibility for our changeable schedules.

Data availability statement. All data from the Atmospheric Tomography mission are openly available and archived in the Oak Ridge National Laboratory Distributed Active Archive Center (ORNL DAAC) at https://doi.org/10.3334/ORNLDAAC/1925.

References

Andreae, M., and Coauthors, 1985: Dimethyl sulfide in the marine atmosphere. *J. Geophys. Res.*, **90**, 12 891–12 900, https://doi.org/10.1029/JD090iD07p12891.

Anenberg, S. C., and Coauthors, 2012: Global air quality and health co-benefits of mitigating near-term climate change through methane and black carbon emission controls. *Environ. Health Perspect.*, **120**, 831–839, https://doi.org/10.1289/ehp.1104301.

Ayers, G., and Coauthors, 1996: The annual cycle of peroxides and ozone in marine air at Cape Grim, Tasmania. *J. Atmos. Chem.*, **23**, 221–252, https://doi.org/10.1007/BF00055155.

Bates, K. H., and Coauthors, 2021: The global budget of atmospheric methanol: New constraints on secondary, oceanic, and terrestrial sources. *J. Geophys. Res. Atmos.*, **126**, e2020JD033439, https://doi.org/10.1029/2020JD033439.

Bates, T., B. Lamb, A. Guenther, J. Dignon, and R. Stoiber, 1992: Sulfur emissions to the atmosphere from natural sources. *J. Atmos. Chem.*, **14**, 315–337, https://doi.org/10.1007/BF00115242.

Bian, H., and Coauthors, 2019: Observationally constrained analysis of sea salt aerosol in the marine atmosphere. *Atmos. Chem. Phys.*, **19**, 10 773–10 785, https://doi.org/10.5194/acp-19-10773-2019.

Bourgeois, I., and Coauthors, 2020: Global-scale distribution of ozone in the remote troposphere from the ATom and HIPPO airborne field missions. *Atmos. Chem. Phys.*, **20**, 10 611–10 635, https://doi.org/10.5194/acp-20-10611-2020.

Brewer, J., and Coauthors, 2020: Evidence for an oceanic source of methyl ethyl ketone to the atmosphere. *Geophys. Res. Lett.*, **47**, e2019GL086045, https://doi.org/10.1029/2019GL086045.

Brock, C. A., and Coauthors, 2019: Aerosol size distributions during the Atmospheric Tomography Mission (ATom): Methods, uncertainties, and data products. *Atmos. Meas. Tech.*, **12**, 3081–3099, https://doi.org/10.5194/amt-12-3081-2019.

——, and Coauthors, 2021: Ambient aerosol properties in the remote atmosphere from global-scale in-situ measurements. *Atmos. Chem. Phys.*, **21**, 152023–152063, https://doi.org/10.5194/acp-21-15023-2021.

Brune, W., and Coauthors, 2020: Exploring oxidation in the remote free troposphere: Insights from Atmospheric Tomography (ATom). *J. Geophys. Res. Atmos.*, **125**, e2019JD031685, https://doi.org/10.1029/2019JD031685.

Charlson, R. J., J. E. Lovelock, M. O. Andreae, and S. G. Warren, 1987: Oceanic phytoplankton, atmospheric sulphur, cloud albedo and climate. *Nature*, **326**, 655–661, https://doi.org/10.1038/326655a0.

Chevallier, F., M. Remaud, C. W. O'Dell, D. Baker, P. Peylin, and A. Cozic, 2019: Objective evaluation of surface-and satellite-driven carbon dioxide atmospheric inversions. *Atmos. Chem. Phys.*, **19**, 14 233–14 251, https://doi.org/10.5194/acp-19-14233-2019.

Clarke, A. D., 1993: Atmospheric nuclei in the Pacific midtroposphere: Their nature, concentration, and evolution. *J. Geophys. Res.*, **98**, 20 633–20 647, https://doi.org/10.1029/93JD00797.

——, and V. N. Kapustin, 2002: A Pacific aerosol survey. Part I: A decade of data on particle production, transport, evolution, and mixing in the troposphere. *J. Atmos. Sci.*, **59**, 363–382, https://doi.org/10.1175/1520-0469(2002)059<0363:APASPI>2.0.CO;2.

——, and ——, 2010: Hemispheric aerosol vertical profiles: Anthropogenic impacts on optical depth and cloud nuclei. *Science*, **329**, 1488–1492, https://doi.org/10.1126/science.1188838.

Crawford, J., and Coauthors, 2004: Relationship between Measurements of Pollution in the Troposphere (MOPITT) and in situ observations of CO based on a large-scale feature sampled during TRACE-P. *J. Geophys. Res.*, **109**, D15S04, https://doi.org/10.1029/2003JD004308.

Crowell, S., and Coauthors, 2019: The 2015–2016 carbon cycle as seen from OCO-2 and the global in situ network. *Atmos. Chem. Phys.*, **19**, 9797–9831, https://doi.org/10.5194/acp-19-9797-2019.

Deeter, M. N., and Coauthors, 2019: Radiance-based retrieval bias mitigation for the MOPITT instrument: The version 8 product. *Atmos. Meas. Tech.*, **12**, 4561–4580, https://doi.org/10.5194/amt-12-4561-2019.

Di Carlo, P., and Coauthors, 2004: Missing OH reactivity in a forest: Evidence for unknown reactive biogenic VOCs. *Science*, **304**, 722–725, https://doi.org/10.1126/science.1094392.

Eastham, S. D., and D. J. Jacob, 2017: Limits on the ability of global Eulerian models to resolve intercontinental transport of chemical plumes. *Atmos. Chem. Phys.*, **17**, 2543–2553, https://doi.org/10.5194/acp-17-2543-2017.

Emmons, L., and Coauthors, 2015: The POLARCAT Model Intercomparison Project (POLMIP): Overview and evaluation with observations. *Atmos. Chem. Phys.*, **15**, 6721–6744, https://doi.org/10.5194/acp-15-6721-2015.

Fiore, A. M., and Coauthors, 2012: Global air quality and climate. *Chem. Soc. Rev.*, **41**, 6663–6683, https://doi.org/10.1039/c2cs35095e.

Fishman, J., C. E. Watson, J. C. Larsen, and J. A. Logan, 1990: Distribution of tropospheric ozone determined from satellite data. *J. Geophys. Res.*, **95**, 3599–3617, https://doi.org/10.1029/JD095iD04p03599.

——, K. Fakhruzzaman, B. Cros, and D. Nganga, 1991: Identification of widespread pollution in the Southern Hemisphere deduced from satellite analyses. *Science*, **252**, 1693–1696, https://doi.org/10.1126/science.252.5013.1693.

——, J. M. Hoell Jr., R. D. Bendura, R. J. McNeal, and V. W. Kirchhoff, 1996: NASA GTE trace a experiment (September–October 1992): Overview. *J. Geophys. Res.*, **101**, 23 865–23 879, https://doi.org/10.1029/96JD00123.

Fleming, Z. L., and Coauthors, 2018: Tropospheric Ozone Assessment Report: Present-day ozone distribution and trends relevant to human health. *Elementa*, **6**, 12, https://doi.org/10.1525/elementa.273.

Fried, A., and Coauthors, 2008: Formaldehyde over North America and the North Atlantic during the summer 2004 INTEX campaign: Methods, observed distributions, and measurement-model comparisons. *J. Geophys. Res.*, **113**, D10302, https://doi.org/10.1029/2007JD009185.

Froyd, K. D., and Coauthors, 2019: A new method to quantify mineral dust and other aerosol species from aircraft platforms using single-particle mass spectrometry. *Atmos. Meas. Tech.*, **12**, 6209–6239, https://doi.org/10.5194/amt-12-6209-2019.

Gaudel, A., and Coauthors, 2018: Tropospheric Ozone Assessment Report: Present-day distribution and trends of tropospheric ozone relevant to climate and global atmospheric chemistry model evaluation. *Elementa*, **6**, 39, https://doi.org/10.1525/elementa.291.

Gelaro, R., and Coauthors, 2017: The Modern-Era Retrospective Analysis for Research and Applications, version 2 (MERRA-2). *J. Climate*, **30**, 5419–5454, https://doi.org/10.1175/JCLI-D-16-0758.1.

Gonzalez, Y., and Coauthors, 2021: Impact of stratospheric air and surface emissions on tropospheric nitrous oxide during ATom. *Atmos. Chem. Phys.*, **21**, 11 113–11 132, https://doi.org/10.5194/acp-21-11113-2021.

Guo, H., and Coauthors, 2021: Heterogeneity and chemical reactivity of the remote troposphere defined by aircraft measurements. *Atmos. Chem. Phys.*, **21**, 13 729–13 746, https://doi.org/10.5194/acp-21-13729-2021.

Hall, S. R., and Coauthors, 2018: Cloud impacts on photochemistry: Building a climatology of photolysis rates from the Atmospheric Tomography mission. *Atmos. Chem. Phys.*, **18**, 16 809–16 828, https://doi.org/10.5194/acp-18-16809-2018.

Hansen, J., M. Sato, R. Ruedy, A. Lacis, and V. Oinas, 2000: Global warming in the twenty-first century: An alternative scenario. *Proc. Natl. Acad. Sci. USA*, **97**, 9875–9880, https://doi.org/10.1073/pnas.170278997.

Heald, C. L., and Coauthors, 2003: Asian outflow and trans-Pacific transport of carbon monoxide and ozone pollution: An integrated satellite, aircraft, and model perspective. *J. Geophys. Res.*, **108**, 4804, https://doi.org/10.1029/2003JD003507.

Helmig, D., D. Tanner, R. Honrath, R. Owen, and D. Parrish, 2008: Nonmethane hydrocarbons at Pico Mountain, Azores: 1. Oxidation chemistry in the North Atlantic region. *J. Geophys. Res.*, **113**, D20S91, https://doi.org/10.1029/2007JD008930.

Hintsa, E. J., and Coauthors, 2021: UAS Chromatograph for Atmospheric Trace Species (UCATS) – A versatile instrument for trace gas measurements on airborne platforms. *Atmos. Meas. Tech.*, **14**, 6795–6819, https://doi.org/10.5194/amt-14-6795-2021.

Hodzic, A., P. S. Kasibhatla, D. S. Jo, C. D. Cappa, J. L. Jimenez, S. Madronich, and R. J. Park, 2016: Rethinking the global Secondary Organic Aerosol (SOA) budget: Stronger production, faster removal, shorter lifetime. *Atmos. Chem. Phys.*, **16**, 7917–7941, https://doi.org/10.5194/acp-16-7917-2016.

——, and Coauthors, 2020: Characterization of organic aerosol across the global remote troposphere: A comparison of ATom measurements and global chemistry models. *Atmos. Chem. Phys.*, **20**, 4607–4635, https://doi.org/10.5194/acp-20-4607-2020.

Hoffmann, E. H., A. Tilgner, R. Schroedner, P. Bräuer, R. Wolke, and H. Herrmann, 2016: An advanced modeling study on the impacts and atmospheric implications of multiphase dimethyl sulfide chemistry. *Proc. Natl. Acad. Sci. USA*, **113**, 11 776–11 781, https://doi.org/10.1073/pnas.1606320113.

Holmes, C. D., M. J. Prather, O. Sovde, and G. Myhre, 2013: Future methane, hydroxyl, and their uncertainties: Key climate and emission parameters for future predictions. *Atmos. Chem. Phys.*, **13**, 285–302, https://doi.org/10.5194/acp-13-285-2013.

IPCC, 2022: *Climate Change 2021: The Physical Science Basis*. V. Masson-Delmotte et al., Eds., Cambridge University Press, in press.

Katich, J. M., and Coauthors, 2018: Strong contrast in remote black carbon aerosol loadings between the Atlantic and Pacific basins. *J. Geophys. Res. Atmos.*, **123**, 13 386–13 395, https://doi.org/10.1029/2018JD029206.

Kirtman, B., and Coauthors, 2013: Near-term climate change: Projections and predictability. *Climate Change 2013: The Physical Science Basis*, T. F. Stocker et al., Eds., Cambridge University Press, 953–1028.

Koenig, T. K., and Coauthors, 2020: Quantitative detection of iodine in the stratosphere. *Proc. Natl. Acad. Sci. USA*, **117**, 1860–1866, https://doi.org/10.1073/pnas.1916828117.

Kulawik, S. S., and Coauthors, 2021: Evaluation of single-footprint AIRS CH4 profile retrieval uncertainties using aircraft profile measurements. *Atmos. Meas. Tech.*, **14**, 335–354, https://doi.org/10.5194/amt-14-335-2021.

Lamarque, J.-F., and Coauthors, 2013: The Atmospheric Chemistry and Climate Model Intercomparison Project (ACCMIP): Overview and description of models, simulations and climate diagnostics. *Geosci. Model Dev.*, **6**, 179–206, https://doi.org/10.5194/gmd-6-179-2013.

Lamb, K., and Coauthors, 2021: Global-scale constraints on light-absorbing anthropogenic iron oxide aerosols. *npj Climate Atmos. Sci.*, **4**, 15, https://doi.org/10.1038/s41612-021-00171-0.

Liu, J., and Coauthors, 2021: Carbon monitoring system flux net biosphere exchange 2020 (CMS-Flux NBE 2020). *Earth Syst. Sci. Data*, **13**, 299–330, https://doi.org/10.5194/essd-13-299-2021.

Liu, S. C., and Coauthors, 1992: A study of the photochemistry and ozone budget during the Mauna Loa observatory photochemistry experiment. *J. Geophys. Res.*, **97**, 10 463–10 471, https://doi.org/10.1029/91JD02298.

Luo, G., F. Yu, and J. M. Moch, 2020: Further improvement of wet process treatments in GEOS-Chem v12.6.0: Impact on global distributions of aerosols and aerosol precursors. *Geosci. Model Dev.*, **13**, 2879–2903, https://doi.org/10.5194/gmd-13-2879-2020.

Lou, S., and Coauthors, 2020: New SOA treatments within the Energy Exascale Earth System Model (E3SM): Strong production and sinks govern atmospheric SOA distributions and radiative forcing. *J. Adv. Model. Earth Syst.*, **12**, e2020MS002266, https://doi.org/10.1029/2020MS002266.

Lu, X., and Coauthors, 2021: Global methane budget and trend, 2010–2017: Complementarity of inverse analyses using in situ (GLOBALVIEWplus CH4 ObsPack) and satellite (GOSAT) observations. *Atmos. Chem. Phys.*, **21**, 4637–4657, https://doi.org/10.5194/acp-21-4637-2021.

Martínez-Alonso, S., and Coauthors, 2020: 1.5 years of TROPOMI CO measurements: Comparisons to MOPITT and ATom. *Atmos. Meas. Tech.*, **13**, 4841–4864, https://doi.org/10.5194/amt-13-4841-2020.

McNeal, R., D. Jacob, D. Davis, and S. Liu, 1998: The NASA Global Tropospheric Experiment: Recent accomplishments and future plans. *IGAC Newsletter*, No. 13, NASA, Boulder, CO, www-air.larc.nasa.gov/missions/tracep/IGAC.htm.

Monks, P. S., L. J. Carpenter, S. A. Penkett, G. P. Ayers, R. W. Gillett, I. E. Galbally, and C. M. Meyer, 1998: Fundamental ozone photochemistry in the remote marine boundary layer: The SOAPEX experiment, measurement and theory. *Atmos. Environ.*, **32**, 3647–3664, https://doi.org/10.1016/S1352-2310(98)00084-3.

Murphy, D. M., and Coauthors, 2018: An aerosol particle containing enriched uranium encountered in the remote upper troposphere. *J. Environ. Radioact.*, **184**, 95–100, https://doi.org/10.1016/j.jenvrad.2018.01.006.

——, and Coauthors, 2019: The distribution of sea-salt aerosol in the global troposphere. *Atmos. Chem. Phys.*, **19**, 4093–4104, https://doi.org/10.5194/acp-19-4093-2019.

——, and Coauthors, 2021: Radiative and chemical implications of the size and composition of aerosol particles in the existing or modified global stratosphere. *Atmos. Chem. Phys.*, **21**, 8915–8932, https://doi.org/10.5194/acp-2020-909.

Myhre, G., and Coauthors, 2013: Anthropogenic and natural radiative forcing. *Climate Change 2013: The Physical Science Basis.* Cambridge University Press, 659–740.

Naik, V., and Coauthors, 2013: Preindustrial to present-day changes in tropospheric hydroxyl radical and methane lifetime from the Atmospheric Chemistry and Climate Model Intercomparison Project (ACCMIP). *Atmos. Chem. Phys.*, **13**, 5277–5298, https://doi.org/10.5194/acp-13-5277-2013.

Nalli, N. R., and Coauthors, 2020: Validation of carbon trace gas profile retrievals from the NOAA-unique combined atmospheric processing system for the cross-track infrared sounder. *Remote Sens.*, **12**, 3245, https://doi.org/10.3390/rs12193245.

Nault, B. A., C. Garland, S. Pusede, P. Wooldridge, K. Ullmann, S. Hall, and R. Cohen, 2015: Measurements of CH3O2NO2 in the upper troposphere. *Atmos. Meas. Tech.*, **8**, 987–997, https://doi.org/10.5194/amt-8-987-2015.

——, and Coauthors, 2021: Chemical transport models often underestimate inorganic aerosol acidity in remote regions of the atmosphere. *Commun. Earth. Environ.*, **2**, 93, https://doi.org/10.1038/s43247-021-00164-0.

Oman, L., J. Ziemke, A. Douglass, D. Waugh, C. Lang, J. Rodriguez, and J. Nielsen, 2011: The response of tropical tropospheric ozone to ENSO. *Geophys. Res. Lett.*, **38**, L13706, https://doi.org/10.1029/2011GL047865.

Prather, M., and Coauthors, 2001: Atmospheric chemistry and greenhouse gases. *Climate Change 2001: The Scientific Basis*, J. Houghton, Ed., Cambridge University Press, 239–287.

——, C. D. Holmes, and J. Hsu, 2012: Reactive greenhouse gas scenarios: Systematic exploration of uncertainties and the role of atmospheric chemistry. *Geophys. Res. Lett.*, **39**, L09803, https://doi.org/10.1029/2012GL051440.

——, and Coauthors, 2017: Global atmospheric chemistry–Which air matters. *Atmos. Chem. Phys.*, **17**, 9081–9102, https://doi.org/10.5194/acp-17-9081-2017.

——, and Coauthors, 2018: How well can global chemistry models calculate the reactivity of short-lived greenhouse gases in the remote troposphere, knowing the chemical composition. *Atmos. Meas. Tech.*, **11**, 2653–2668, https://doi.org/10.5194/amt-11-2653-2018.

Quinn, P. K., and T. S. Bates, 2011: The case against climate regulation via oceanic phytoplankton sulphur emissions. *Nature*, **480**, 51–56, https://doi.org/10.1038/nature10580.

Read, K., and Coauthors, 2012: Multiannual observations of acetone, methanol, and acetaldehyde in remote tropical Atlantic air: Implications for atmospheric OVOC budgets and oxidative capacity. *Environ. Sci. Technol.*, **46**, 11 028–11 039, https://doi.org/10.1021/es302082p.

Rickly, P. S., L. Xu, J. D. Crounse, P. O. Wennberg, and A. W. Rollins, 2021: Improvements to a laser-induced fluorescence instrument for measuring SO2 – Impact on accuracy and precision. *Atmos. Meas. Tech.*, **14**, 2429–2439, https://doi.org/10.5194/amt-14-2429-2021.

Rollins, A. W., and Coauthors, 2016: A laser-induced fluorescence instrument for aircraft measurements of sulfur dioxide in the upper troposphere and lower stratosphere. *Atmos. Meas. Tech.*, **9**, 4601–4613, https://doi.org/10.5194/amt-9-4601-2016.

Schill, G., and Coauthors, 2020: Widespread biomass burning smoke throughout the remote troposphere. *Nat. Geosci.*, **13**, 422–427, https://doi.org/10.1038/s41561-020-0586-1.

Schum, S. K., B. Zhang, K. Džepina, P. Fialho, C. Mazzoleni, and L. R. Mazzoleni, 2018: Molecular and physical characteristics of aerosol at a remote free troposphere site: Implications for atmospheric aging. *Atmos. Chem. Phys.*, **18**, 142017–142036, https://doi.org/10.5194/acp-18-14017-2018.

Schwarz, J., and Coauthors, 2013: Global-scale seasonally resolved black carbon vertical profiles over the Pacific. *Geophys. Res. Lett.*, **40**, 5542–5547, https://doi.org/10.1002/2013GL057775.

Scovronick, N., H. Adair-Rohani, and N. Borgford-Parnell, 2015: *Reducing Global Health Risks through Mitigation of Short-Lived Climate Pollutants: Scoping Report for Policymakers.* World Health Organization, 140 pp.

Shindell, D., J. Kuylenstierna, F. Raes, V. Ramanathan, E. Rosenthal, and S. Terry, 2011: Integrated assessment of black carbon and tropospheric ozone: Summary for decision makers. World Meteorological Organization, 38 pp., http://119.78.100.173/C666/handle/2XK7JSWQ/10118.

——, and Coauthors, 2012a: Simultaneously mitigating near-term climate change and improving human health and food security. *Science*, **335**, 183–189, https://doi.org/10.1126/science.1210026.

——, and Coauthors, 2012b: Radiative forcing in the ACCMIP historical and future climate simulations. *Atmos. Chem. Phys.*, **12**, 21 105–21 210, https://doi.org/10.5194/acp-13-2939-2013.

Singh, H., W. Brune, J. Crawford, F. Flocke, and D. J. Jacob, 2009: Chemistry and transport of pollution over the Gulf of Mexico and the Pacific: Spring 2006 INTEX-B campaign overview and first results. *Atmos. Chem. Phys.*, **9**, 2301–2318, https://doi.org/10.5194/acp-9-2301-2009.

St. Clair, J. M., A. K. Swanson, S. A. Bailey, and T. F. Hanisco, 2019: CAFE: A new, improved nonresonant laser-induced fluorescence instrument for airborne in situ measurement of formaldehyde. *Atmos. Meas. Tech.*, **12**, 4581–4590, https://doi.org/10.5194/amt-12-4581-2019.

Stephens, B. B., E. J. Morgan, J. D. Bent, R. F. Keeling, A. S. Watt, S. R. Shertz, and B. C. Daube, 2021: Airborne measurements of oxygen concentration from the surface to the lower stratosphere and pole to pole. *Atmos. Meas. Tech.*, **14**, 2543–2574, https://doi.org/10.5194/amt-14-2543-2021.

Strode, S. A., and Coauthors, 2018: Forecasting carbon monoxide on a global scale for the ATom-1 aircraft mission: Insights from airborne and satellite observations and modeling. *Atmos. Chem. Phys.*, **18**, 10 955–10 971, https://doi.org/10.5194/acp-18-10955-2018.

Thames, A. B., and Coauthors, 2020: Missing OH reactivity in the global marine boundary layer. *Atmos. Chem. Phys.*, **20**, 4013–4029, https://doi.org/10.5194/acp-20-4013-2020.

Travis, K. R., and Coauthors, 2016: Why do models overestimate surface ozone in the Southeast United States? *Atmos. Chem. Phys.*, **16**, 13 561–13 577, https://doi.org/10.5194/acp-16-13561-2016.

——, and Coauthors, 2020: Constraining remote oxidation capacity with ATom observations. *Atmos. Chem. Phys.*, **20**, 7753–7781, https://doi.org/10.5194/acp-20-7753-2020.

Tsigaridis, K., and Coauthors, 2014: The AeroCom evaluation and intercomparison of organic aerosol in global models. *Atmos. Chem. Phys.*, **14**, 10 845–10 895, https://doi.org/10.5194/acp-14-10845-2014.

Velders, G. J., D. W. Fahey, J. S. Daniel, M. McFarland, and S. O. Andersen, 2009: The large contribution of projected HFC emissions to future climate forcing. *Proc. Natl. Acad. Sci. USA*, **106**, 10 949–10 954, https://doi.org/10.1073/pnas.0902817106.

Veres, P. R., and Coauthors, 2020: Global airborne sampling reveals a previously unobserved dimethyl sulfide oxidation mechanism in the marine atmosphere. *Proc. Natl. Acad. Sci. USA*, **117**, 4505–4510, https://doi.org/10.1073/pnas.1919344117.

Voulgarakis, A., and Coauthors, 2013: Analysis of present day and future OH and methane lifetime in the ACCMIP simulations. *Atmos. Chem. Phys.*, **13**, 2563–2587, https://doi.org/10.5194/acp-13-2563-2013.

Wang, S., and Coauthors, 2019: Atmospheric acetaldehyde: Importance of air-sea exchange and a missing source in the remote troposphere. *Geophys. Res. Lett.*, **46**, 5601–5613, https://doi.org/10.1029/2019GL082034.

——, and Coauthors, 2020: Global atmospheric budget of acetone: Air-sea exchange and the contribution to hydroxyl radicals. *J. Geophys. Res. Atmos.*, **125**, e2020JD032553, https://doi.org/10.1029/2020JD032553.

Watson, C. E., J. Fishman, and H. G. Reichle Jr., 1990: The significance of biomass burning as a source of carbon monoxide and ozone in the southern hemisphere tropics: A satellite analysis. *J. Geophys. Res.*, **95**, 16 443–16 450, https://doi.org/10.1029/JD095iD10p16443.

Watson-Parris, D., and Coauthors, 2019: In situ constraints on the vertical distribution of global aerosol. *Atmos. Chem. Phys.*, **19**, 11 765–11 790, https://doi.org/10.5194/acp-19-11765-2019.

West, J. J., A. M. Fiore, L. W. Horowitz, and D. L. Mauzerall, 2006: Global health benefits of mitigating ozone pollution with methane emission controls. *Proc. Natl. Acad. Sci. USA*, **103**, 3988–3993, https://doi.org/10.1073/pnas.0600201103.

Williamson, C. J., and Coauthors, 2019: A large source of cloud condensation nuclei from new particle formation in the tropics. *Nature*, **574**, 399–403, https://doi.org/10.1038/s41586-019-1638-9.

Wofsy, S. C., 2011: HIAPER Pole-to-Pole Observations (HIPPO): Fine-grained, global-scale measurements of climatically important atmospheric gases and aerosols. *Philos. Trans. Roy. Soc. London*, **A369**, 2073–2086, https://doi.org/10.1098/rsta.2010.0313.

Wolfe, G. M., and Coauthors, 2019: Mapping hydroxyl variability throughout the global remote troposphere via synthesis of airborne and satellite formaldehyde observations. *Proc. Natl. Acad. Sci. USA*, **116**, 11 171–11 180, https://doi.org/10.1073/pnas.1821661116.

Wu, R., S. Wang, and L. Wang, 2015: New mechanism for the atmospheric oxidation of dimethyl sulfide. The importance of intramolecular hydrogen shift in a CH3SCH2OO radical. *J. Phys. Chem.*, **119A**, 112–117, https://doi.org/10.1021/jp511616j.

Yang, Y., M. Shao, X. Wang, A. C. Nölscher, S. Kessel, A. Guenther, and J. Williams, 2016: Towards a quantitative understanding of total OH reactivity: A review. *Atmos. Environ.*, **134**, 147–161, https://doi.org/10.1016/j.atmosenv.2016.03.010.

Young, P., and Coauthors, 2013: Pre-industrial to end 21st century projections of tropospheric ozone from the Atmospheric Chemistry and Climate Model Intercomparison Project (ACCMIP). *Atmos. Chem. Phys.*, **13**, 2063–2090, https://doi.org/10.5194/acp-13-2063-2013.

Yu, P., and Coauthors, 2019: Efficient in-cloud removal of aerosols by deep convection. *Geophys. Res. Lett.*, **46**, 1061–1069, https://doi.org/10.1029/2018GL080544.

Zaelke, D., 2013: Primer on short-lived climate pollutants. Institute for Governance and Sustainable Development, 72 pp., www.igsd.org/documents/PrimeronShort-LivedClimatePollutantsElectronicVersion.pdf.

Zeng, L., and Coauthors, 2020: Global measurements of brown carbon and estimated direct radiative effects. *Geophys. Res. Lett.*, **47**, e2020GL088747, https://doi.org/10.1029/2020GL088747.

Zhang, Y., O. R. Cooper, A. Gaudel, A. M. Thompson, P. Nédélec, S.-Y. Ogino, and J. J. West, 2016: Tropospheric ozone change from 1980 to 2010 dominated by equatorward redistribution of emissions. *Nat. Geosci.*, **9**, 875–879, https://doi.org/10.1038/ngeo2827.

Zhu, L., and Coauthors, 2020: Validation of satellite formaldehyde (HCHO) retrievals using observations from 12 aircraft campaigns. *Atmos. Chem. Phys.*, **20**, 122329–122345, https://doi.org/10.5194/acp-20-12329-2020.